POLITECNICO DI TORINO
Repository ISTITUZIONALE

Electrophoretic co-deposition of Fe2O3 and Mn1,5Co1,5O4: Processing and oxidation performance of Fe-doped Mn-Co coatings for solid oxide cell interconnects

Original
Electrophoretic co-deposition of Fe2O3 and Mn1,5Co1,5O4: Processing and oxidation performance of Fe-doped Mn-Co coatings for solid oxide cell interconnects / Zanchi, E.; Talic, B.; Sabato, A. G.; Molin, S.; Boccaccini, A. R.; Smeacetto, F.. - In: JOURNAL OF THE EUROPEAN CERAMIC SOCIETY. - ISSN 0955-2219. - ELETTRONICO. - 39:13(2019), pp. 3768-3777. [10.1016/j.jeurceramsoc.2019.05.024]

Availability:
This version is available at: 11583/2737177 since: 2019-06-25T13:59:26Z

Publisher:
Elsevier Ltd

Published
DOI:10.1016/j.jeurceramsoc.2019.05.024

Terms of use:

This article is made available under terms and conditions as specified in the corresponding bibliographic description in the repository

Publisher copyright
Elsevier postprint/Author's Accepted Manuscript

© 2019. This manuscript version is made available under the CC-BY-NC-ND 4.0 license
http://creativecommons.org/licenses/by-nc-nd/4.0/.The final authenticated version is available online at:
http://dx.doi.org/10.1016/j.jeurceramsoc.2019.05.024

(Article begins on next page)

24 April 2024

Elsevier Editorial System(tm) for Journal of the European Ceramic Society

Manuscript Draft

Manuscript Number: JECS-D-19-00722R1

Title: Electrophoretic co-deposition of Fe2O3 and Mn1,5Co1,5O4: processing and oxidation performance of Fe-doped Mn-Co coatings for solid oxide cell interconnects

Article Type: Full Length Article

Keywords: Electrophoretic deposition; Ceramic coating; Solid oxide cell

Corresponding Author: Ms. Elisa Zanchi, MSc

Corresponding Author's Institution: Politecnico di Torino

First Author: Elisa Zanchi, MSc

Order of Authors: Elisa Zanchi, MSc; Belma Talic, Dr.; Antonio G Sabato, Dr.; Sebastian Molin, Dr.; Aldo R Boccaccini, Prof. Dr.-Ing. habil.; Federico Smeacetto, Prof.

Abstract: Fe-doped Mn1,5Co1,5O4 coatings on Crofer22APU were processed by an electrophoretic co-deposition method and the corrosion resistance was tested at 750°C up to 2000 hours.
The "in-situ" Fe-doping of the manganese cobalt spinel was achieved by electrophoretic co-deposition of Mn1,5Co1,5O4 and Fe2O3 powders followed by a two-step reactive sintering treatment. The effects on the coating properties of two different Fe-doping levels (5 and 10 wt.% respectively) and two different temperatures of the reducing treatment (900 and 1000°C) are discussed. Samples with Fe-doped coatings demonstrated a lower parabolic oxidation rate and thinner oxide scale in comparison with both the undoped Mn1,5Co1,5O4 spinel coating and bare Crofer 22 APU. The best corrosion protection was achieved with the combined effect of Fe-doping and a higher temperature of the reducing step at 1000°C.

POLITECNICO
DI TORINO
Department of Applied Science and Technology

PhD student
Elisa Zanchi, MSc

Torino, May 14th, 2019

To the Editor of *Journal of the European Ceramic Society*

OBJECT: Revision of the paper "Electrophoretic co-deposition of Fe_2O_3 and $Mn_{1,5}Co_{1,5}O_4$: processing and oxidation performance of Fe-doped Mn-Co coatings for solid oxide cell interconnects"

Dear Editor,

We have considered the Reviewers' comments to our paper, enclosed in your e-mail message of 7th of May.

First of all, we wish to thank you and the reviewer for the attention dedicated to the revision of the paper. We have reviewed the paper taking into account the Reviewer's comments. The answers to each comment are presented in the "Detailed Response to Reviewer Comments" document. The changes in the manuscript are highlighted in red type.

We sincerely hope that this work can be published on your Journal to have a wide diffusion through the Scientific Community.

Thank you for your kind attention.

Best Regards,

Elisa Zanchi,

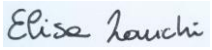

on behalf of all Authors

Department of Applied Science and Technology
Politecnico di Torino Corso Duca degli Abruzzi, 24 – 10129 Torino – Italia
tel: +39 011.090.4756
elisa.zanchi@polito.it

Reviewers' comments:

Editor: The referee has recognised that interesting and original results have been put forward in your paper. There are, however, some recommendations for revision that need attention before I can accept the paper for publication.

Reviewer #1: This paper presents the synthesis of Fe-doped Mn-Co coatings deposited on the Crofer 22 APU steel, which was performed via the electrophoretic co-deposition of Fe2O3 and Mn1.5Co1.5O4 - an approach that is unique and unprecedented as far as literature is concerned. The aim of the conducted study was to modify the surface of the Crofer 22 APU ferritic stainless steel in such a way as to optimize its performance in an intermediate-temperature solid oxide fuel cell (IT-SOFC) stack. In order to assess the suitable of the steel they had modified, the authors performed extensive physicochemical investigations of the steel/coating layered system, evaluating its oxidation resistance with the use of adequate research methods. Overall, I found the obtained results very interesting, and in my opinion the experimental work and the way it is presented are both very good. The manuscript can be strongly recommended for publication after addressing the issues below:

1. Taking into account the high rank of the Journal of the European Ceramic Society, it would also be worth including the results of electrical conductivity studies, assuming they had been performed for the investigated systems - this parameter is a determiner of their suitability for use in the production of fuel cells. If the authors plan to publish such results in another paper that will discuss this in more detail, this comment can just be ignored.

   We agree with the reviewer on the importance of the electrical conductivity studies; to this purpose, a further paper will be dedicated to a detailed analysis of the long-term electrical conductivity performance of these systems.

2. Introduction: What was the rationale for the choice of two (and not more) spinels with different iron content? It would also be worth mentioning this in the part where the authors describe their objectives.

   We decided to introduce only low percentages of iron oxide to the EPD suspensions in the view of the Z potential results of Fe_2O_3 and $Mn_{1.5}Co_{1.5}O_4$ powders, in order to not affect the deposition process and to avoid an inversion of the deposition direction. Furthermore, 5 and 10 wt.% of Fe_2O_3 doping precursor amounts were chosen in order to avoid the risk of reaching the maximum solubility of Fe in the pristine $Mn_{1.5}Co_{1.5}O_4$ spinel.
   We also verified that variations of EPD suspension composition smaller than 5% could be difficult to control on the laboratory scale.
   As suggested by the reviewer, we added the following sentence at page 6 in Section 3.1: “These experiments validated the rationale for the choice of the two different iron contents in the spinel; 5 and 10 wt.% of Fe_2O_3 doping precursor amounts were chosen in order to maintain a cathodic deposition process and to avoid the risk of reaching the maximum solubility of Fe in the pristine $Mn_{1.5}Co_{1.5}O_4$ spinel.”

3. Section 3.2, page 7, lines 46-47: The authors state that the grain size distribution was bimodal. It would be best if they included a diagram showing an example of this distribution.

   This observation is related to the comment of Figure 3d of the manuscript, where we wanted to show that performing the reducing treatment at higher temperature only partially promotes the coarsening of the metallic particles.
   We recognise that the highlighted expression is too specific in this case; therefore, it has been replaced at page 7 in Section 3.2 by “However, the coarsening of the metallic particles did not affect the

homogeneity of the metallic phase in the reduced coating; an appreciable fraction of smaller particles (< 0.1 µm) is still present.".

4. Section 3.2, page 9, lines 41-44: There are two issues with this statement. It seems to be in contradiction to what is presented in Fig. 5, in which I can clearly discern the growth of an intermediate reaction layer. To confirm this, EDS line scan (and not point) analysis should be performed. In addition, if I understand correctly and the phrase "compared to that already reported after the reducing treatment" refers to literature reports, then the corresponding bibliographical items should be cited.

   As pointed out by the reviewer, after the second sintering step, the coatings and the chromia scale reacted forming an intermediate reaction layer. We performed EDX line scans for every samples, collecting similar plots to the one attached below (Fig 1). It can be noted that the thickness of both the chromia scale and the reaction layer is very limited (< 1 µm), so that reporting the measurements in the paper could have been misleading (also considering the sensitivity of the instrument). For this reason, we decided not to include EDX line scans of coatings after sintering in the paper. On the contrary we reported EDX line scans of aged coatings (Figure 11 in the Manuscript) because the thickening of the oxide scale due to high-temperature oxidation allowed to determine precise values with acceptable standard deviations. Moreover, as far as the protection against oxidation given by the coatings is concerned, we decided to focus on the oxide scale evolution during aging at 750°C and not on the one formed during the sintering process.

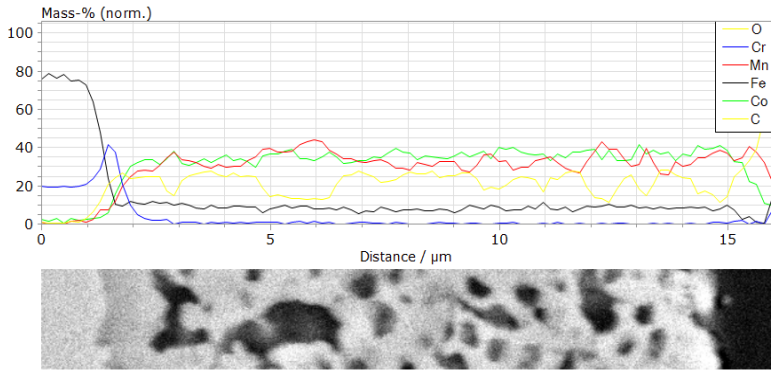

Fig 1: EDX line scan of 10FeMCO_R1000 coating after the two-step sintering.

   The phrase "compared to that already reported after the reducing treatment" refers to the comment of Figure 3 (showing the cross section of coatings after the first sintering step). Indeed, the analysis of EDX line scans allowed us to verify that the second heat treatment did not cause a remarkable thickening of the oxide scale compared to what already measured on coatings after the first heat treatment, as described in Section 3.2, page 7.
   We admit that the points highlighted by the reviewer can be misleading; it has been modified in the revised manuscript at page 9 in Section 3.2 to "As reported in Figure 5, only trace amounts of Cr (< 0.4 at.%) were detected in the coatings (marked areas). Comparing Figure 3 and Figure 5, it is apparent that both the oxide and metallic phases of the coating reacted with the chromia scale on the steel surface during the oxidizing treatment; the total thickness of the chromia scale and the intermediate layer between it and the coating was evaluated by EDX line scans, resulting < 1 µm for all the studied cases."

5. Table 2: The authors obviously wanted to clearly present the parabolic oxidation rate constant by using a common multiplier (10^(-15)) for all of the rows. However, kp,m = value x 10^(-n) [units], while the header row for the third column reads "kp,m x 10^(-15)". In practice that would make kp,m = value /

10^(-15). In my opinion the header for this column should either read "kp,m x 10^15" or ""kp,m / 10^(-15)".

The error has been corrected. The common multiplier 10^{-15} has been added to every row in Table 2 to avoid misunderstanding.

6. Figure 6: The units used for the time axis in these two plots should be the same, i.e. hours.

   The units used in Figure 6 have been adapted to hours for both the plots.

7. Section 3.4, text fragment starting in line 60 of page 12 and ending in line 2 of the page 13: I would not use "somewhat" to describe the degree to which the Cr vaporization rate is reduced by the outer manganese-chromium spinel layer when compared to chromia. This is quite precisely given in the literature on the subject.

   The reported expression was a typing error and has been deleted in the manuscript.

*Manuscript_revised
Click here to view linked References

Electrophoretic co-deposition of Fe_2O_3 and $Mn_{1,5}Co_{1,5}O_4$: processing and oxidation performance of Fe-doped Mn-Co coatings for solid oxide cell interconnects

E. Zanchi[1,*], B. Talic[2], A. G. Sabato[1], S. Molin[3], A. R. Boccaccini[4], F. Smeacetto[5]

1. Department of Applied Science and Technology, Politecnico di Torino, Corso Duca degli Abruzzi 24, 10129 Torino, Italy
2. Department of Energy Conversion and Storage, Technical University of Denmark, DTU Risø Campus, Frederiksborgvej 399, DK-4000 Roskilde, Denmark
3. Faculty of Electronics, Telecommunications and Informatics, Gdańsk University of Technology, ul. Narutowicza 11/12, 80-233 Gdańsk, Poland
4. Department of Materials Science and Engineering, University of Erlangen-Nuremberg, Cauerstr. 6, 91058 Erlangen, Germany
5. Department of Energy, Politecnico di Torino, Corso Duca degli Abruzzi 24, 10129 Torino, Italy

*Corresponding author at: Department of Applied Science and Technology, Politecnico di Torino, Corso Duca degli Abruzzi 24, 10129 Torino, Italy.
E-mail address: elisa.zanchi@polito.it

Abstract

Fe-doped $Mn_{1,5}Co_{1,5}O_4$ coatings on Crofer22APU were processed by an electrophoretic co-deposition method and the corrosion resistance was tested at 750°C up to 2000 hours.

The “in-situ” Fe-doping of the manganese cobalt spinel was achieved by electrophoretic co-deposition of $Mn_{1,5}Co_{1,5}O_4$ and Fe_2O_3 powders followed by a two-step reactive sintering treatment. The effects on the coating properties of two different Fe-doping levels (5 and 10 wt.% respectively) and two different temperatures of the reducing treatment (900 and 1000°C) are discussed. Samples with Fe-doped coatings demonstrated a lower parabolic oxidation rate and thinner oxide scale in comparison with both the undoped $Mn_{1,5}Co_{1,5}O_4$ spinel coating and bare Crofer 22 APU. The best corrosion protection was achieved with the combined effect of Fe-doping and a higher temperature of the reducing step at 1000°C.

Keywords: Electrophoretic deposition; Ceramic coating; Solid oxide cell

1. Introduction

Solid Oxide Fuel Cells (SOFCs) are energy conversion devices that produce electricity through electrochemical reactions between a fuel and an oxidant. They are considered a promising technology towards the development of low-emission energy production methods [1,2]. To produce a usable power output, several cells can be

stacked together and connected by interconnects. The interconnects provide an electrical connection between the cells and act as a physical barrier to prevent direct combination of the fuel and the oxidant [3]. SOFCs working temperatures lay in the range 500-850 °C [4].

Previous studies have established chromia-forming ferritic stainless steels (FSSs) as the most suitable interconnect material for SOFC stacks, due to their high electrical conductivity, gas tightness, thermo-mechanical stability and thermal expansion coefficient (TEC) match (11-12.5 × 10^{-6} K^{-1} [5]) with the other SOFC materials (ca. 10.5-12.5 × 10^{-6} K^{-1} [6]). FSSs also offer a better mechanical strength, easier manufacturing and cost effectiveness compared to the previously used ceramic interconnect materials [7–9]. Different heat-resistant FSSs have been developed specially for SOFC applications, among which, Crofer 22 APU (ThyssenKrupp VDM) is the most widely used [10]. A high Cr content (22-24%) in the alloy ensures the formation of a continuous and well adherent Cr_2O_3 scale, which provides good resistance against high-temperature corrosion [11,12].

However, degradation of the FSSs interconnect under the stacks operating conditions is still a major issue for the durability of SOFC stacks. Long term service leads to excessive thickening of the chromia scale, which results in Cr depletion from the steel, lowering its corrosion resistance [13], as well as a decline of the electrical performance [14]. Even if the thermally-grown Cr_2O_3 scale behaves as a semiconductor, its conductivity (0.6–16 × 10^{-2} Scm^{-1} at 800 °C [15]) is much lower than that of the steel (around 90 × 10^{2} Scm^{-1} [10]). In addition, the Cr_2O_3 can react with oxygen and H_2O in the oxidizing atmosphere to form volatile Cr^{6+}-compounds (such as CrO_3 and $CrO_2(OH)_2$), which migrate to the cathode/electrolyte interface and degrade the electrochemical performances of the cell (so-called cathode poisoning) [16,17].

Applying a protective coating on the steel has been established as a promising approach to extend the interconnect life and mitigate cathode poisoning [18–20]. Among the different coating materials investigated [21–23], the $(Mn,Co)_3O_4$ spinel family has been shown to be particularly promising. The $(Mn,Co)_3O_4$ spinels have a satisfactory electrical conductivity, TEC match with other SOFC materials and good adhesion to the steel [24–28]. Moreover, it has been demonstrated that $(Mn,Co)_3O_4$ coatings reduce both chromium outward diffusion and the steel corrosion rate [29–35]. Among the different compositions that may be expressed by the generic formula $(Mn,Co)_3O_4$, the greatest attention is given to $MnCo_2O_4$ and $Mn_{1.5}Co_{1.5}O_4$ (which at room temperature exhibits a dual-phase microstructure of the cubic $MnCo_2O_4$ and tetragonal Mn_2CoO_4).

The spinel coatings have been deposited by various techniques such as: slurry and spray deposition [24,29–31], screen printing [34,35], physical vapour deposition [36], thermal spray and thermal oxidation [37,38] and plasma spray [39]. Among the deposition methods, electrophoretic deposition (EPD) has gained great interest, thanks to its simple and adaptable set-up, versatility for materials employed and coatings morphology, cost-effectiveness, low-energy demand, as well as the suitability for industrial applications [40]. EPD of cobalt-manganese spinel coatings has already demonstrated promising results in terms of green density, adhesion and protective effect on the steel substrate [25,41–43]. Molin et al. [33] tested $(Mn,Co)_3O_4$

spinel coatings obtained by sputtering, thermal co-evaporation and EPD under SOFC relevant conditions for 5000 h and concluded that the EPD coating was the most satisfactory in terms of low Area Specific Resistance (ASR).

When EPD or other slurry-based methods are used, a subsequent heat-treatment is generally required to sinter the deposited powders and form a dense and continuous layer on the steel. The coating density has been shown to have a strong influence on the steel corrosion rate and chromium volatilization [34,44]. In this regard, the advantages of a two-step sintering procedure, which is made up of a heat treatment in reducing atmosphere followed by a heat treatment in an oxidizing atmosphere, have already been reported [42,45]. For example Bobruk et al. [41] showed that reduction at 1000°C in H_2/Ar and re-oxidation at 900 °C in air (both for 2 h) was the optimal sintering procedure for a $MnCo_2O_4$ coating deposited by EPD. The added cost of the reducing step is justified by the better protective performance of the coatings [46].

Currently, many studies are focusing on the possibility to improve the $(Mn,Co)_3O_4$ spinel further by transition metal doping, in particularly with Fe or/and Cu [44,47–55]. Since the coating properties are strongly affected by the preparation procedure, there is considerable scatter in the literature results. Nevertheless, there is evidence that Fe-doping reduces the TEC of $(Mn,Co)_3O_4$, thus improving the thermo-mechanical compatibility with the substrate. For example, Talic et al. [49] found that the TEC decreased with Fe-doping from 14.4 × 10^{-6} K^{-1} for $MnCo_2O_4$ to 11.0 × 10^{-6} K^{-1} for $MnCo_{1.5}Fe_{0.5}O_4$. In terms of oxidation resistance, it is not clear whether Fe-doping has a beneficial effect. Talic et al. [44,48] reported that the ASR and oxidation kinetics of $MnCo_{1.7}Fe_{0.3}O_4$ were similar to those of $MnCo_2O_4$, while Bednarz et al. [55] concluded that Fe-modified coatings exhibit an improved high-temperature oxidation resistance in comparison with the $Mn_{1.5}Co_{1.5}O_4$ coating.

Up to now, Fe-doped manganese-cobaltite spinel has been synthetized before coating deposition, following what can be called an “ex-situ” procedure, requiring time-consuming, energy demanding and sequential processes such as: spray pyrolysis [44,48,49], high energy ball milling [50], solid state synthesis [54], and sol-gel processes [52,55]. A novel prospective offered by the EPD technique is the possibility to achieve doped Mn-Co spinel coatings by a single-step co-deposition of different oxides. This “in-situ” approach allows to reduce the processing time and cost. Optimization of the sintering technique is even more relevant when different oxides are co-deposited since they need to react between each other and reach a homogenous microstructure. Recently, Molin et al. [56] investigated the effectiveness of the EPD method to obtain “in-situ” Cu-doped manganese-cobalt spinel by co-depositing $Mn_{1,5}Co_{1,5}O_4$ and CuO in a single-step and subjecting the coating to a two-step reactive sintering treatment (2h in Ar-4%/H_2 at 900°C and 2h in air at 900°C). The Cu-doped coatings demonstrated satisfactory results in terms of composition, ASR and corrosion resistance.

In the present work the possibility of using the EPD technique to co-deposit $Mn_{1,5}Co_{1,5}O_4$ spinel and Fe_2O_3 powders on Crofer 22 APU is investigated. The achievement of the Fe-doping of the spinel by a two-step reactive sintering is assessed as well. The protective performance of the in-situ-Fe-modified coatings is evaluated and compared against a pristine $Mn_{1,5}Co_{1,5}O_4$ coating and the bare Crofer

22 APU steel through a study of the oxidation kinetics at 750 °C up to 2000 h. The effects on the coating properties of two different Fe-doping levels and two different temperatures of the reducing treatment are discussed.

2. Experimental

Crofer 22 APU (Cr=23 wt.%, Mn=0.45 wt.%, La= 0.1 wt.%, Ti=0.06 wt.%, Si and Al <0.05 wt.%, Fe=Bal.) provided by Thyssen Krupp was chosen as substrate for the deposition. Coupons with the size of 20 × 20 mm^2 were cut from a 0.3 mm thick steel plate and a Ø3 mm hole was punched in one of the corners, to allow for hanging in the furnace during the oxidation test. Before deposition the coupons were cleaned in acetone and ethanol for 10 min each. Commercially available $Mn_{1.5}Co_{1.5}O_4$ (MCO) spinel powder from Fuelcellmaterials and Fe_2O_3 powder from Fluka were used for the co-deposition.

The EPD suspensions were prepared using a solution containing 60 vol.% of ethanol and 40 vol.% of deionized water as dispersant medium; the powders were added to reach a total solid loading of 37.5 gL^{-1}. This formulation is based on suspensions previously optimized and tested for both MCO deposition [25,33] and MCO/CuO co-deposition [56]. Three different suspensions were prepared, containing 0 wt.%, 5 wt.% and 10 wt.% of Fe_2O_3, in the following labelled MCO, 5FeMCO and 10FeMCO, respectively. Before deposition, each suspension was sonicated for 10 s in an ultrasonic bath and mixed for 10 s with a magnetic stirrer, both for 3 times in a row. While not in use, the suspensions were kept on the magnetic stirrer.

The deposition was carried out using a three-electrode configuration: it consisted of two steel counter-electrodes fixed at 1 cm from the sample, which was placed in the middle in order to coat both surfaces. A constant voltage of 50 V was applied for 20 s.

Dynamic light scattering (DLS) was used to determine the size distributions and Z potential of MCO and Fe_2O_3 powders in 60EtOH/40H_2O solution by a Malvern Zetasizer Nano Series instrument. Due to limitations of the technique [57], measurements were performed for MCO and Fe_2O_3 separately and on diluted suspensions: concentration was fixed at 37.5 × 10^{-3} gL^{-1} (0.001 of that used for depositions). Suspensions were sonicated for 20 min and let stabilize for 20 min without any stirring, before being inserted in the instrument cuvette. Measurements were repeated six time in order to average the results; the equilibration time of the instrument electrodes was chosen to be 120 s. The pH value of the 60EtOH/40H_2O solution lays in the neutral range (pH=7.5); no other pH variations were considered.

After drying at room temperature, the coated coupons were sintered by a two-step procedure. The first heat treatment in reducing atmosphere (Ar/H_2 4%) was performed at 900°C for 2h. It was followed by the second sintering step in oxidizing atmosphere (static air) at 900 °C for 2 h. An additional set with 10FeMCO coating was prepared changing the temperature of the first treatment to 1000°C (in the following labelled 10FeMCO_R1000) and keeping unchanged all the other sintering parameters. For each sample variant (amount of Fe and reducing temperature) 5 samples were prepared and tested. Samples labels and main features are summarized in Table 1. The theoretical compositions of the coatings have been

calculated assuming that the MCO and Fe_2O_3 powders homogeneously deposit and react fully to form the spinel structure during sintering.

The oxidation kinetics of the coated steel and bare Crofer 22 APU was evaluated by thermo-gravimetric test, exposing 4 samples for each kind in static air at 750°C in a chamber furnace for a total time of 2000 h. The furnace was cooled every 250 h (cooling rate: 120 °C/h) and the sample weighted (XS205 Mettler Toledo scale, 10^{-5} g accuracy) to evaluate the mass gain after every thermal cycle. The measured mass gain reflects the oxygen uptake due to oxide scale formation and growth, assuming no other processes that could cause a change in weight (i.e. evaporation, spallation) occur [58]. After 1000 h and 2000 h of aging one coupon of each type was taken out of the furnace for characterization.

The crystal structure of the coatings was studied by X-Ray diffraction (XRD) using a Bruker D8 instrument with Cu-Kα radiation; the patterns were recorded at room temperature on rotating samples in a 2θ configuration from 10° to 70°. XRD patterns for coatings after the reducing step were collected in grazing incidence angle mode using a PanAlytical X'Pert Pro PW 3040/60 Philips diffractometer with Cu-Kα radiation from 10°-70°. All the coupons were subsequently embedded in epoxy resin (Struers, Denmark) and polished to reveal the cross section. Morphological and compositional characterization of the cross sections was carried out by a scanning electron microscope (SEM, Zeiss Merlin) equipped with an energy dispersive X-Ray analyser (EDX, Bruker). The coatings porosity was evaluated by a graphical method using the IMAGEJ software [59]. Three SEM images of the same magnification from different regions of each sample were analysed to calculate a mean porosity value. EDX analysis was used to evaluate the thickness of the thermally grown oxide scale; at least three representative EDX line-scans from different areas of each sample were considered.

Table 1: Samples nomenclature, EPD suspension compositions, sintering procedures and theoretical coatings compositions.

Sample name	EPD suspension	Two-step sintering	Coating theoretical composition
MCO	100wt.% $Mn_{1.5}Co_{1.5}O_4$	900°C, 2h, Ar/H_2 900°C, 2h, air	$Mn_{1,5}Co_{1,5}O_4$
5FeMCO	95wt.% $Mn_{1.5}Co_{1.5}O_4$ 5wt.% Fe_2O_3	900°C, 2h, Ar/H_2 900°C, 2h, air	$Mn_{1,43}Co_{1,43}Fe_{0,14}O_4$
10FeMCO	90wt.% $Mn_{1.5}Co_{1.5}O_4$ 10wt.% Fe_2O_3	900°C, 2h, Ar/H_2 900°C, 2h, air	$Mn_{1,35}Co_{1,35}Fe_{0,30}O_4$
10FeMCO_R1000	90wt.% $Mn_{1.5}Co_{1.5}O_4$ 10wt.% Fe_2O_3	1000°C, 2h, Ar/H_2 900°C, 2h, air	$Mn_{1,35}Co_{1,35}Fe_{0,30}O_4$

3. Results and discussion

3.1. Study of the co-deposition process

Although the theoretical discussion of the EPD process is not the purpose of the present study, a series of experiments was carried out to characterize the suspensions used for the co-depositions, aiming at obtaining understanding about the correlation between suspension characteristics and coating properties.

Figure 1 reports FE-SEM images of MCO (a) and Fe_2O_3 (b) used for the EPD co-depositions. The $Mn_{1.5}Co_{1.5}O_4$ powder shows fragments with irregular shape and broad size distribution (ranging from 150 to 750 nm, d_{50}=634 nm). Iron oxide is composed of rounded particles with a diameter of 50 to 90 nm (d_{50}=75 nm), thus considerably smaller than those of MCO.

Zeta potential results obtained by DLS analysis of the two studied suspensions (37.5 10^{-3} gL^{-1} in 60EtOh/40H_2O, pH=7.5) resulted to be +12.7 mV for MCO and -9.9 mV for Fe_2O_3.
Most studies in the field of MCO coatings deposited by EPD have mainly focused on morphological and electrical characterization of the coated steel substrates, while few data deal with the characterization of these powders in the EPD suspensions. For example, Smeacetto et. al [25] has reported that manganese-cobalt oxide undergoes cathodic deposition (positive surface charge) in the same solution here investigated. Moreover, Mikolajczyk et al. [60] has reported that Fe_2O_3 nanoparticles develop a zeta potential equal to -18.1 mV in liquid media (pH=7.5).
The fact that Fe_2O_3 particles develop a negative surface charge in ethanol/water solution was here verified by depositing on steel coupons a EPD suspension of iron oxide (37.5 gL^{-1}, EtOH/H_2O 60/40 vol.%); the anodic deposition was obtained by applying 70 V for 20s, thus forming a homogeneous layer on the positive electrode.

Considering the powders particle size, their relative concentration and the zeta potential data, a co-deposition mechanism is here proposed and reported schematically in Figure 1c. The Fe_2O_3 particles are associated by electrostatic interaction with those of MCO, which are generally larger. The deposition resulted cathodic due to the electrostatic interactions between opposite surface charges and to the greater concentration of MCO particles in the suspensions. A similar co-deposition mechanism of particles with opposite surface charge has already been proposed by Corni et. al [61].
These experiments validated the rationale for the choice of the two different iron contents in the spinel; 5 and 10 wt.% of Fe_2O_3 doping precursor amounts were chosen in order to maintain a cathodic deposition process and to avoid the risk of reaching the maximum solubility of Fe in the pristine $Mn_{1.5}Co_{1.5}O_4$ spinel.

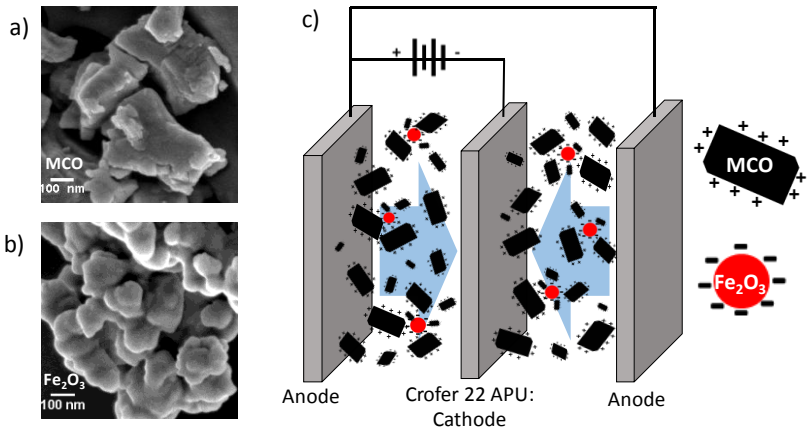

Figure 1: FE-SEM images of MCO (a) and Fe_2O_3 (b) powders used for EPD and schematization of the proposed co-deposition mechanism in the three-electrode set up (c).

3.2. Characterization of the as-prepared coatings

Figure 2 shows the XRD patterns collected on the coating surfaces after the first heat treatment in reducing atmosphere (Ar/H_2). For all samples, the deposited $Mn_{1.5}Co_{1.5}O_4$ spinel was reduced to MnO and metallic Co. The coatings obtained by co-depositing the spinel powder and Fe_2O_3 do not show any residual iron oxide peaks, suggesting successful reduction at both 900 and 1000 °C in Ar/H_2. The 10FeMCO and 10FeMCO_R1000 coatings exhibit similar patters after reduction, both having an additional peak at around 45°, which may be assigned to the formation of the intermetallic compound $Co_{0.7}Fe_{0.3}$. The same phase was not detected in the 5FeMCO pattern, probably due to the smaller Fe addition. A further effect observed in all the Fe-modified samples is the slight shift of the metallic Co peaks towards lower 2θ angles compared to the Co peaks of the pristine MCO (see excerpt in Figure 2a).

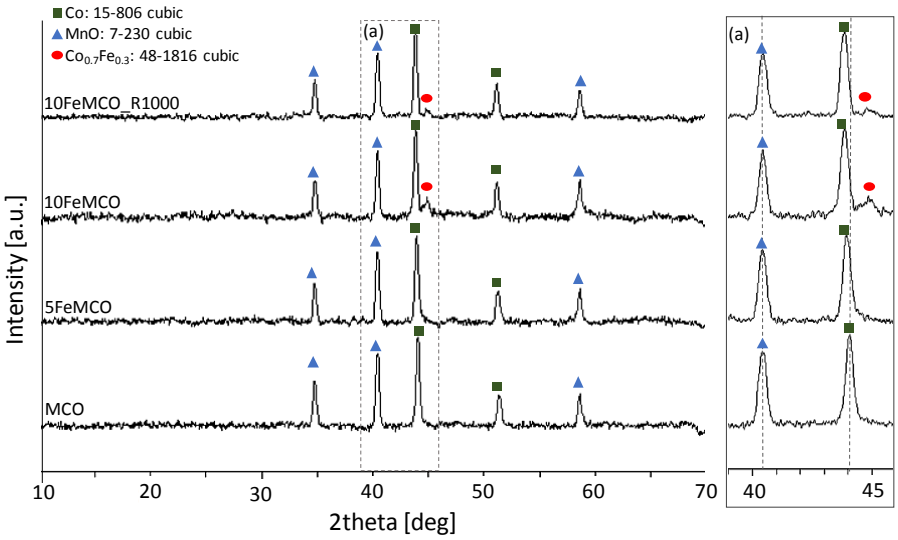

Figure 2: X-Ray diffraction patterns of the pristine and Fe-doped coatings after the reducing step. Patterns are normalized to the intensity of the highest peak. (a) *Excerpt of patterns between 39° and 46°.*

SEM images comparing the cross section of the pristine and Fe-doped coatings after the reduction heat treatment are provided in Figure 3. Here, the bright particles in the coating layer correspond to metallic Co, while the darker contrast particles correspond to MnO. In the MCO coating (Figure 3a), the Co particles show a broad size distribution (0.1-1 µm), with irregular shapes (both spherical and elongated). From Figure 3b, it can be observed that the 5FeMCO coating contains a greater fraction of smaller (≈0.1 µm) metallic Co particles that are well distributed in the coating. With a higher Fe addition (10FeMCO, Figure 3c) the largest metallic particles become coarser (0.2-0.3 µm), but still a high fraction of small (< 0.1 µm) metallic particles can be observed.

For the coating reduced at a higher temperature (10FeMCO_R1000, Figure 3d), the metallic particles appear even coarser, due to the higher temperature of the heat treatment enhancing agglomeration/sintering. However, the coarsening of the metallic particles did not affect the homogeneity of the metallic phase in the reduced coating; an appreciable fraction of smaller particles (< 0.1 µm) is still present. The heat-treatment at 1000°C led to a thicker oxide scale (0.4±0.2 µm) than the one at 900°C (0.2±0.1 µm). Moreover, it is apparent that the higher temperature enhanced the wettability of the metallic particles onto the Cr_2O_3 layer (Figure 3d).

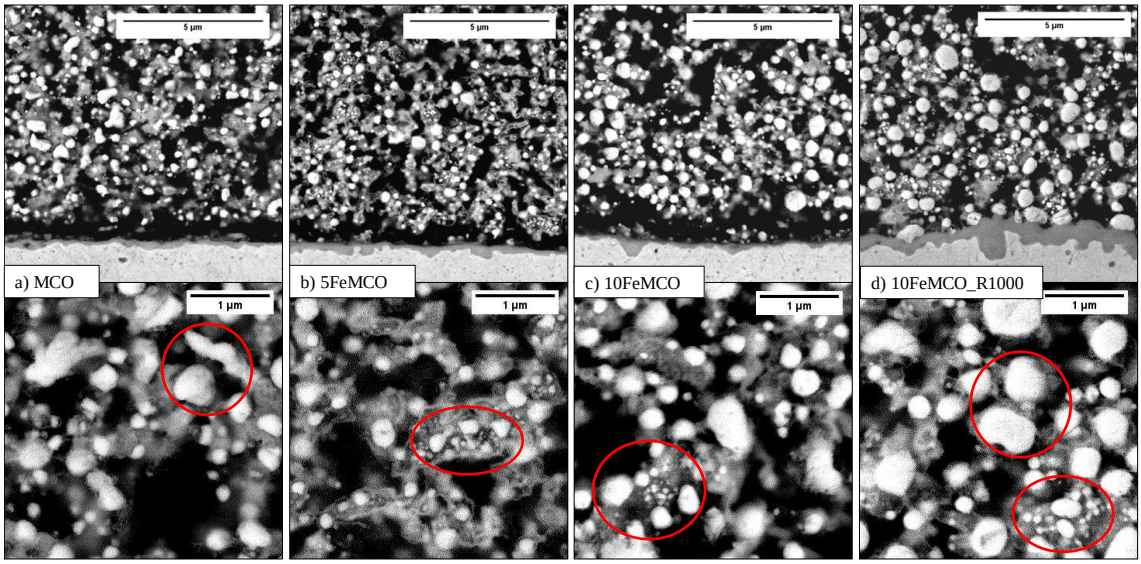

Figure 3: Cross section SEM (backscatter electron mode) images of the coatings after the reduction heat treatment.

The XRD patterns of the coating surfaces after the re-oxidizing step of the sintering heat treatment are shown in Figure 4. All of the patterns exhibit peaks belonging to both the cubic $MnCo_2O_4$ and tetragonal Mn_2CoO_4 spinel phases, thus proving that the spinel structure is re-formed after the re-oxidizing step. No Fe_2O_3 peaks are visible in the patterns of any of the Fe-doped coatings. However, comparing the patters of MCO, 5FeMCO and 10FeMCO, a gradual shift of the cubic phase peaks towards lower 2θ angles with the increasing amount of Fe-doping can be noted. The peak shift can be explained by an increased cubic lattice parameter due to the larger ionic radii of Fe compared to Co. In addition, the relative intensity of the peaks belonging to the tetragonal phase decreases with increasing Fe content, suggesting that Fe-doping stabilizes the cubic spinel structure. The same observations were made by authors in [49] and [50], where the Fe-doping of $MnCo_2O_4$ was achieved through "ex-situ" techniques. The results here demonstrate that Fe-doped MCO spinels can be achieved by electrophoretic co-deposition of $Mn_{1.5}Co_{1.5}O_4$ and Fe_2O_3. No differences are visible between the spectra of 10FeMCO and 10FeMCO_R1000, thus suggesting that the higher reducing temperature did not affect the spinel structure.

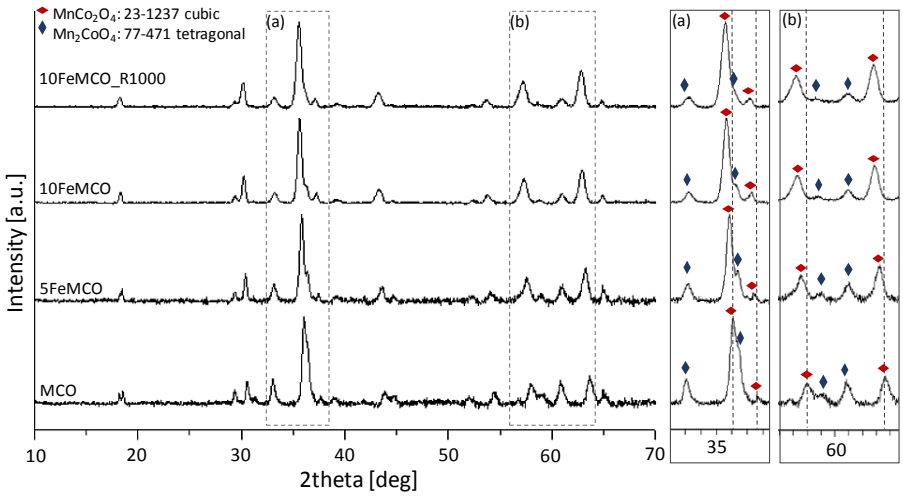

Figure 4: X-Ray diffraction patterns of sintered (reduced and re-oxidized) coatings. Patterns are normalized to the intensity of the highest peak. (a) *Excerpt of patterns between 33 and 38°. (b) Excerpt between 56 and 64°.*

Figure 5 shows SEM cross sectional images of the coatings after the re-oxidizing step. The thickness of all the coatings was measured between 11 and 14 µm. All coatings appear to be well-adherent to the steel and no cracks were observed at the steel/coating interfaces. The porosity of the coatings reduced at 900 °C (reported in Figure 5) decreased slightly with increasing Fe-doping, from 27.5 % for MCO to 24.5 % for 10FeMCO. However, since these differences are close to the standard deviations (respectively: 4.9% for MCO, 5.3% for 5FeMCO and 3.8% for 10FeMCO), it cannot be concluded whether Fe-doping actually is promoting the densification (which is consistent with previous studies [48,50]). The higher temperature of the reducing step had a more pronounced effect on densification, decreasing the porosity of the FeMCO_R1000 coating to only 18.0% (with a standard deviation of 3.5%).

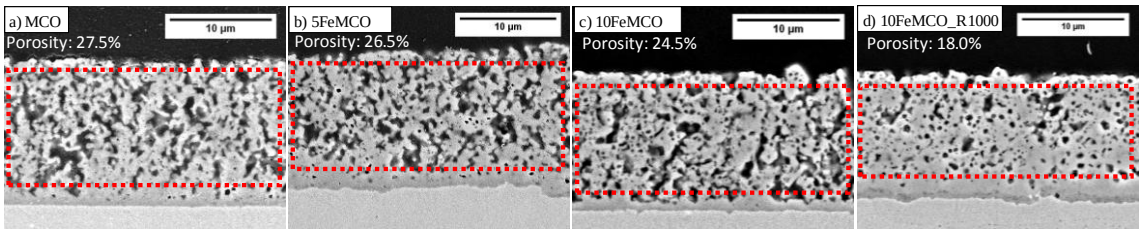

EDS	Mn	Co	Fe	Cr	O
at.%	23.4	22.0	0.7	0.2	53.7
Comp.	$(Mn_{1.52}Co_{1.43}Fe_{0.04}Cr_{0.01})O_4$				

EDS	Mn	Co	Fe	Cr	O
at.%	22.6	19.9	2.5	0.4	54.6
Comp.	$(Mn_{1.50}Co_{1.32}Fe_{0.16}Cr_{0.02})O_4$				

EDS	Mn	Co	Fe	Cr	O
at.%	19.4	19.5	4.6	0.3	56.2
Comp.	$(Mn_{1.33}Co_{1.33}Fe_{0.32}Cr_{0.02})O_4$				

EDS	Mn	Co	Fe	Cr	O
at.%	19.4	19.8	4.4	0.2	56.2
Comp.	$(Mn_{1.33}Co_{1.35}Fe_{0.31}Cr_{0.01})O_4$				

Figure 5: Cross section SEM (secondary electron) images of the coatings after sintering and the mean porosity determined by image analysis. The semi-quantitative EDX results in at. % were collected from the regions marked in red. The composition (Comp.) is calculated on the base of cations fractions, assuming the coatings are stoichiometric spinel oxides.

The elemental distribution of the coatings was investigated by EDX analysis and the average composition of each coating is given in Figure 5. The compositions were calculated on the basis of cations fractions, assuming that the coatings are stoichiometric spinel oxides, i.e. $(A,B)_3O_4$. The Co/Mn ratio is close to 1 for all of the coatings, as expected from to the initial spinel powder composition ($Mn_{1.5}Co_{1.5}O_4$). The slight Mn enrichment measured for MCO and 5FeMCO could be due to Mn diffusion from the alloy. The composition of the Fe-doped coatings is very close to the nominal (reported in Table 1), confirming that the chosen EPD parameters were appropriate to ensure an effective and homogeneous co-deposition of the two powders. As reported in Figure 5, only trace amounts of Cr (< 0.4 at.%) were detected in the coatings (marked areas). Comparing Figure 3 and Figure 5, it is apparent that both the oxide and metallic phases of the coating reacted with the chromia scale on the steel surface during the oxidizing treatment; the total thickness of the chromia scale and the intermediate layer between it and the coating was evaluated by EDX line scans, resulting < 1 µm for all the studied cases.

3.3. Oxidation kinetics

The mass gain of uncoated and spinel coated Crofer 22 APU measured during discontinuous oxidation at 750°C for a total time of 2000 h is reported in Figure 6a. Each point represents the average of 3 to 4 samples of the same kind. The final mass gain after 2000 h of oxidation is summarized in Table 2. The mass gain measurements show that the MCO coating reduces the final mass gain in comparison with bare Crofer 22 APU and that the Fe-doped coatings further decrease the oxygen uptake. There is no apparent effect of increasing the Fe-content from 5FeMCO to 10FeMCO. The highest reduction in oxygen uptake is achieved by the Fe-doped

coating reduced at 1000°C during the sintering treatment (10FeMCO_R1000). This sample exhibited a final mass gain of 0.14 mg cm^{-2}, corresponding to one third of that of the bare steel.

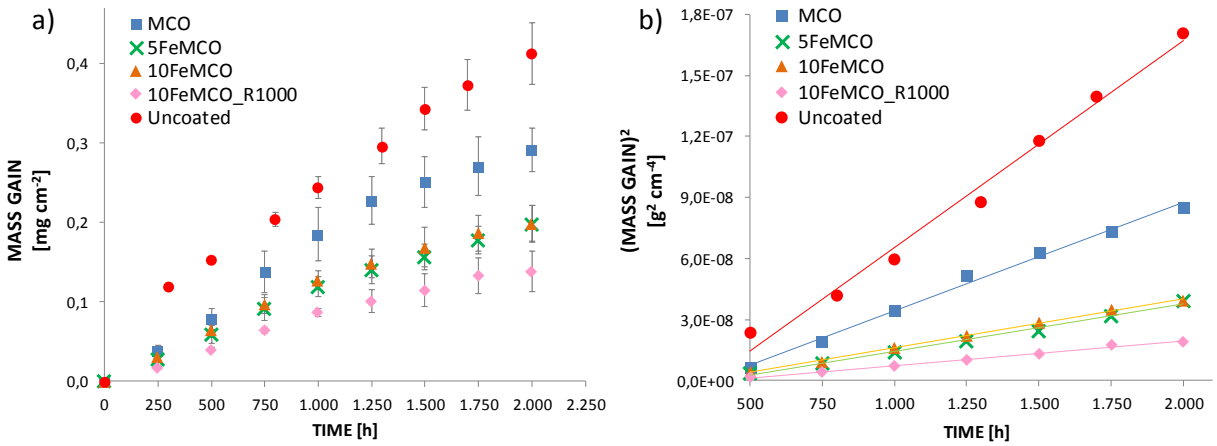

Figure 6: (a) Mass gain of coated and bare Crofer 22 APU during cyclic oxidation at 750 °C in air (0-2000 h). Error bars are equal to one standard deviation. (b) Parabolic rate plot with linear trend lines (500-2000 h).

Table 2: Mass gain after 2000 h aging at 750 °C, parabolic oxidation rate derived from Figure 6b and calculated oxide scale thickness (after 2000 h aging).

Sample	**Mass gain [mg cm^{-2}]**	**$k_{p,m}$ [g^2 cm^{-4} s^{-1}]**	**Oxide scale [µm]**
Uncoated Crofer 22 APU	0.41 ± 0.05	26.9 × 10^{-15}	2.5 ± 0.3
MCO	0.29 ± 0.03	14.5 × 10^{-15}	1.8 ± 0.1
5FeMCO	0.20 ± 0.02	6.6 × 10^{-15}	1.2 ± 0.1
10FeMCO	0.20 ± 0.02	6.6 × 10^{-15}	1.2 ± 0.1
10FeMCO_R1000	0.14 ± 0.03	3.3 × 10^{-15}	0.8 ± 0.2

It is important to note that the mass gain measurements do not reflect the differences in oxide scale thickness before the oxidation test at 750 °C. As seen in Figures 3 and 5, sintering of the spinel coatings leads to oxide scale formation, which is not included in Figure 6a. The bare Crofer 22 APU coupons were tested in the as-received state and were thus not pre-oxidized before the oxidation test at 750 °C. Therefore, the comparison of the mass gain results alone may be an oversimplification and a better comparison of the different samples may be achieved by examining the oxidation kinetics. Figure 6b shows the gravimetric results plotted in parabolic units (g^2 cm^{-4}) as a function of time (s), in accordance with the following equation [62]:

$$\left(\frac{\Delta m}{A}\right)^2 = k_{p,m} \cdot t + C \qquad (1)$$

where Δm is the measured mass gain [g] at a certain aging time (t) [s], A is the sample area [cm^2], C is an integration constant and $k_{p,m}$ is the parabolic rate constant [g^2 cm^{-4} s^{-1}]. $k_{p,m}$ corresponds to the slope of the straight lines in Figure 6b. In the parabolic regime, the oxidation reactions are controlled by lattice diffusion of cations (M^{n+}) and anions (O^{2-}) across the oxide scale [62]. In order to neglect the contribution of the initial transient period and only take into account the steady state growth of the oxide scale, only data from 500 to 2000 h were considered. The calculated values for $k_{p,m}$ are provided in Table 2. The linear fit to the parabolic equation is satisfactory for all the samples (R^2 > 0,99 for the coated steel and R^2 > 0,98 for the bare steel). We note that

the data for the bare Crofer 22 APU fits slightly better to two linear segments, one from 500 to 1300 h ($k_{p,m}$ = 22.5 × 10^{-15} g^2 cm^{-4} s^{-1}) and one from 1300 to 2000 h ($k_{p,m}$ = 32.4 × 10^{-15} g^2 cm^{-4} s^{-1}), indicating a change in the oxidation kinetics with time. A similar time dependence of the oxidation rate of Crofer 22 APU has been reported previously [48].

The application of the 5FeMCO and the 10FeMCO coatings leads to a comparable reduction in $k_{p,m}$ compared to the pristine MCO coating (from 14.5 to 6.6 × 10^{-15} [g^2 cm^{-4} s^{-1}]); which confirms the beneficial effect of the Fe-doping in terms of oxidation resistance. Increasing the doping level from 5 to 10 wt.% does not give any added beneficial effect. The oxidation rate is further reduced by increasing the temperature of the reducing step from 900 °C to 1000 °C ($k_{p,m}$ decreased from 6.6 to 3.3 × 10^{-15} g^2 cm^{-4} s^{-1}). These results suggest that, under the operating conditions adopted by this test, a Crofer 22 APU interconnect coated with 10FeMCO_R1000 could have an eight times longer lifetime than the bare steel.

Assuming the mass gain can be entirely attributed to the oxygen uptake related to forming the Cr_2O_3 scale, the oxide layer thickness can be calculated from the following expression [48,62]:

$$\tau_{Cr_2O_3} = \frac{MW_{Cr_2O_3}}{48 \cdot \rho_{Cr_2O_3}} \cdot \left(\frac{\Delta m}{A}\right) \qquad (3)$$

where τ is the Cr_2O_3 thickness, ρ is its density (5.21 g cm^{-3}), *MW* is its molar weight (152 g mol^{-1}), 48 is a factor for converting the oxygen mass in the Cr_2O_3 (i.e. 16 × 3) and $\frac{\Delta m}{A}$ is the mass gain at 2000 h. The obtained values are reported in Table 2. Considering these results, doping with Fe reduces the oxide scale thickness by 0.6 µm compared to a MCO coating, and increasing the sintering temperature reduces the oxide scale thickness further by 0.4 µm. The critical oxide scale thickness of Crofer 22 APU, before spallation due to TEC mismatch, was previously estimated to be 11.4 µm [63]. According to the obtained oxidation rate constants (reported in Table 2), the oxide scale thickness after 40000h (typical SOFC lifetime target) will be considerably lower than the critical thickness for all of the applied coatings (MCO: 8.8 µm; 5FeMCO: 5.9 µm; 10FeMCO: 5.9 µm; 10FeMCO_R1000: 4.2 µm), but not for the bare Crofer 22 APU (11.9 µm).

3.4. Characterization of the aged coatings

Samples from the oxidation kinetics test were characterized by X-Ray diffraction and SEM/EDX after 1000 and 2000 h aging at 750 °C. Figure 7 shows the X-Ray diffraction patterns of all the studied coatings after 2000 h of aging. The diffraction patterns are very similar to those after sintering (Figure 4), demonstrating the coatings stability over time. As after sintering, both the cubic and tetragonal spinel were detected and Fe-doping appears to stabilize the former (the same trend in the shift of the cubic phase can be appreciated). Increasing the Fe-doping level, the relative intensity of the peaks ascribed to the tetragonal phase is lower than the ones corresponding to the cubic one.

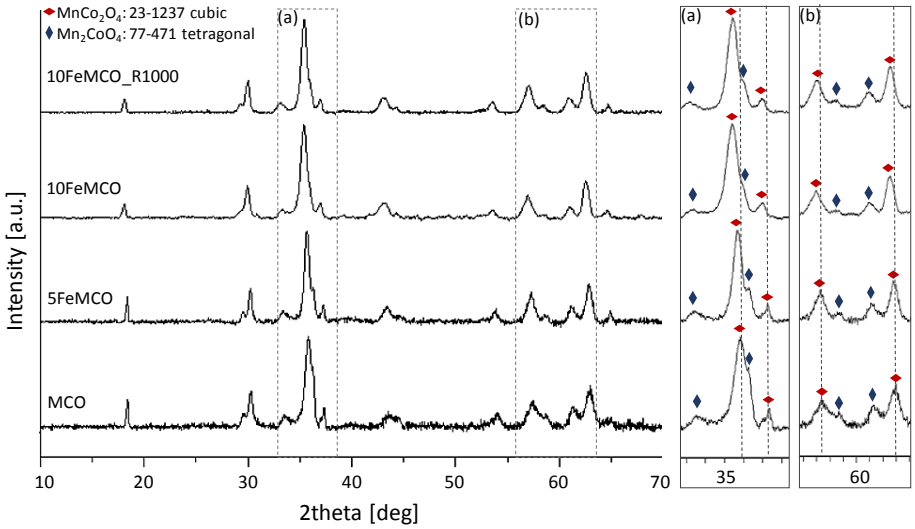

Figure 7: X-Ray diffraction patterns of coatings aged for 2000 h at 750°C. The intensities have been normalized to the highest intensity peak of each pattern. (a) Excerpt of patterns between 33 and 38°. (b) Excerpt between 56 and 64°.

SEM cross sections of samples aged for 1000 and 2000 h are shown in Figure 8 and Figure 9, respectively. In all cases, no cracks could be observed at the coating/steel interface, thus confirming the good thermo-mechanical compatibility between Crofer 22 APU and the produced coatings, despite the thermal cycling every 250h (cooling down for weighting of the samples). After oxidation at 750°C the coatings appear generally denser compared to after sintering (cf. Figure 5), possibly due to slight diffusion of metallic elements (i.e. Mn, Fe, Cr) from the steel.

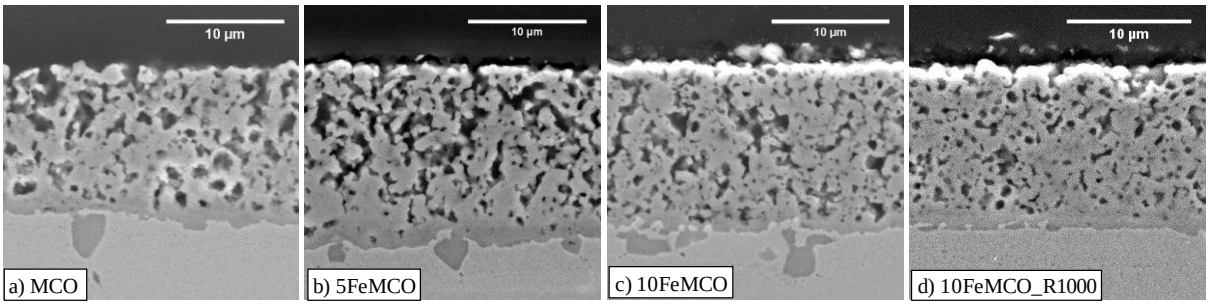

Figure 8: FE-SEM cross section images of the coatings after 1000 h aging at 750°C

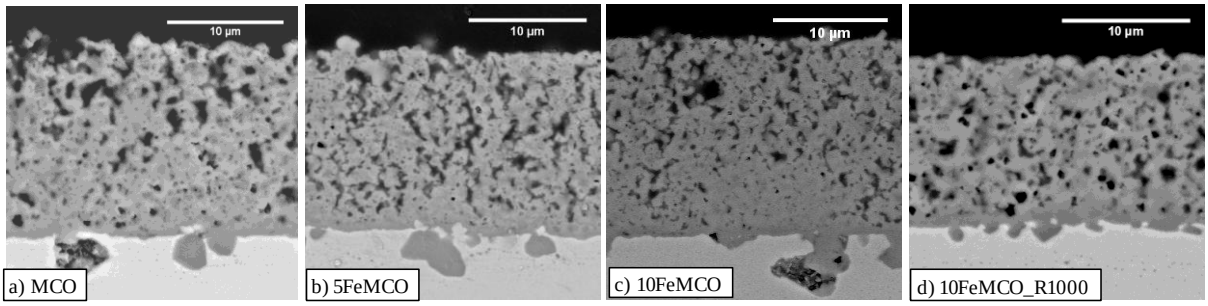

Figure 9: FE-SEM cross section images of the coatings after 2000 h at 750°C.

From Figure 8 and Figure 9 it can also be observed that all coatings that had been reduced at 900°C showed several sub-scale oxides, generally increasing in number and size from 1000 to 2000 h aging. Their average composition was determined by EDX as: Cr= 25 at.%, Mn=13 at.%, O= 60% and traces of Fe and Co. Manganese is

added to the alloy to form an outer $(Mn,Cr)_3O_4$ layer that has been shown to reduce Cr vaporization of bare Crofer 22 APU during oxidation [64]. When a coating is applied on the steel, Mn cations can either migrate through the chromia scale toward the coating [65] or form the Mn-Cr sub-scale nodules (shown in Figure 8 and Figure 9). Here, the second option is observed, indicating that the outward diffusion of Mn is slower than the inward transport of oxygen.

Figure 8d and Figure 9d show representative images of the 10FeMCO_R1000 samples after oxidation. In this case, the sub-scale nodules have smaller dimensions and generally do not extend far into the steel substrate. In a study about Crofer 22 APU pre-oxidation [66], authors outlined that the $(Mn,Cr)_3O_4$ sub-scale nodules preferentially form at the alloy grain boundaries and it was shown that performing a pre-oxidation heat treatment of the steel at higher temperature (i.e. 1000 °C instead of 900 °C) promotes the increase of the grain size and thus fewer sub scale nodules. These evidences well explain the different morphology of samples reduced at 900 °C and 1000 °C.

An EDX map of the 10FeMCO_R1000 sample cross section after 2000 h aging at 750 °C is shown in Figure 10. The Mn, Fe and Co maps (Figure 10 b, c and d) demonstrate that the element distribution is still homogeneous at the end of the oxidation test; the oxide scale is thin and Cr is well confined in it, as shown in Figure 10 e. Comparing Figure 10 b and e, the formation of sub-scale $(Mn,Cr)_3O_4$ can be identified. Figure 10 a reports the average element distribution in the central part of the coating (marked area) and the composition calculated on the basis of the cations fraction. Compared to the EDX results from the as sintered coatings (Figure 5), there is no sign of Fe migration from the steel and the Cr diffusion is limited. However, the Mn/Co ratio (equal to 1.1) has slightly increased during aging. This can be explained by a decrease in cobalt due to evaporation and/or an increase in manganese by diffusion from the steel substrate during aging. The latter would promote coating densification.

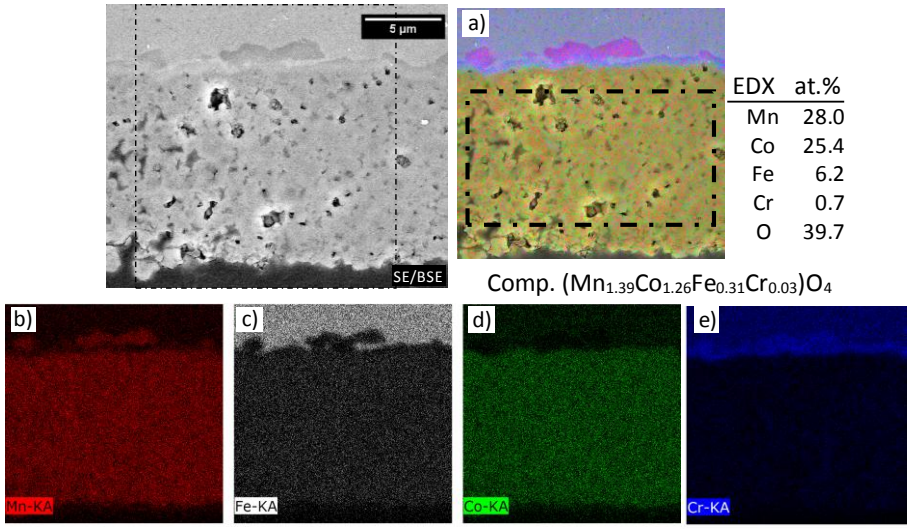

Figure 10: Cross section EDX mapping of 10FeMCO_R1000 sample after 2000 h at 750°C and EDX semi-quantitative results in at. % collected on the marked region in a). The composition (Comp.) is calculated on the base of cations fractions, assuming the coatings are stoichiometric spinel oxides.

The oxide scale thickness of every set of samples after 2000 h aging at 750 °C was determined from the analysis of EDX linescans, as illustrated in Figure 11. The images in Figure 11 correspond to the 5FeMCO coating on Crofer 22 APU and are representative for the other samples as well. The oxide scale thickness was irregular across the steel-coating interface (for example: 0.9 µm Figure 11a and 0.6 µm in Figure 11b). The presence of an inter-diffusion zone between the coating and the chromia scale can be observed in all cases.

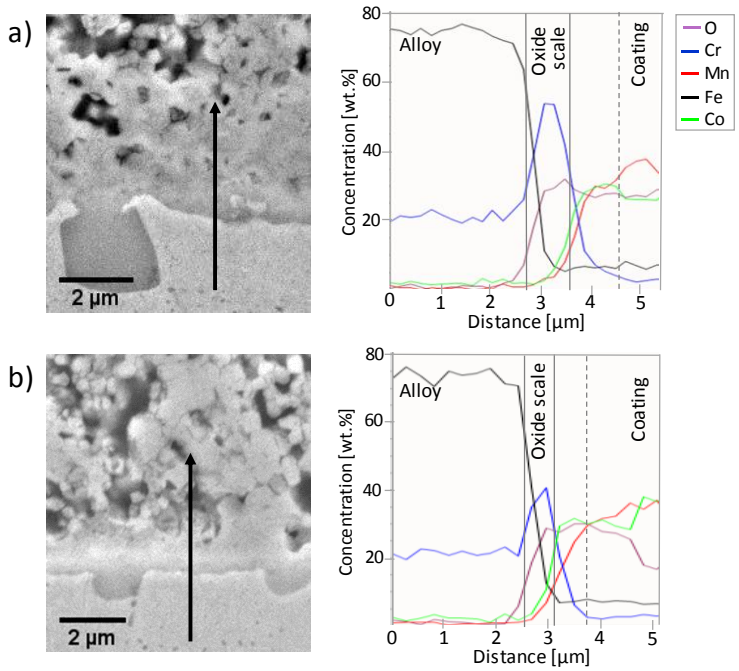

Figure 11: a) and b) EDX linescans along two different areas of the 5FeMCO coated Crofer 22 APU oxidized for 2000 h at 750°C in air.

Table 3 reports the average oxide scale thickness of all coated samples aged for 2000 h, compared to the results calculated from the oxidation mass gain (see section 3.2). According to the measurements, the Cr_2O_3 scale on Crofer 22 APU is on average thicker with the MCO coating compared to any Fe-doped coatings. This result is in line with the lower mass gain exhibited by Fe-doped samples and suggests a beneficial effect of Fe-doping in reducing the growth of the chromia scale. Comparing the measured oxide scale thickness with that calculated from the mass gain shows that for all samples reduced at 900°C (MCO, 5FeMCO and 10FeMCO) the difference between the calculated and the measured oxide scale is on average 0.5 µm. This difference may be assigned to the growth of sub-scale $(Mn,Cr)_3O_4$ nodules (see Figure 8 and Figure 9). In case of the 10FeMCO_R1000 sample, the correspondence between the measured and calculated oxide scale thickness confirms the lower degree of internal oxidation observed.

According to both the measured oxide scale thickness and the mass gain, the 10FeMCO_R1000 coating provides the best protection against oxidation. This can be explained by two factors: 1) the higher coating density reduces the oxygen partial pressure at the oxide scale surface [41,44] and 2) a pre-oxidation effect of the steel substrate, as discussed in [66,67].

Table 3: Measured (from EDX) and calculated (from mass gain) oxide scale thickness of each sample after 2000 h aging at 750°C

Sample	Oxide scale [µm]	
	Measured	**Calculated**
MCO	1.1 ± 0.1	1.8 ± 0.1
5FeMCO	0.8 ± 0.1	1.2 ± 0.1
10FeMCO	0.6 ± 0.2	1.2 ± 0.1
10FeMCO_R1000	0.7 ± 0.2	0.8 ± 0.2

4. Conclusions

This work has demonstrated the possibility of achieving in-situ-Fe-doping of manganese cobalt spinel by electrophoretic co-deposition of $Mn_{1,5}Co_{1,5}O_4$ and Fe_2O_3 followed by a two-step reactive sintering treatment. XRD analysis confirmed that Fe_2O_3 was deposited and completely reduced. Diffraction patterns after re-oxidation showed a mixture of cubic and tetragonal spinel, with Fe stabilizing the former. After 2000 h aging at 750°C, the XRD patterns were unchanged, confirming the high thermal stability of the obtained materials. EDX analysis demonstrated that the coating compositions were close to the nominal values (i.e. $Mn_{1,43}Co_{1,43}Fe_{0,14}O_4$ for the 5FeMCO suspension and $Mn_{1,35}Co_{1,35}Fe_{0,30}O_4$ for the 10FeMCO suspension) even after long-term aging. Therefore, EPD is proposed as an effective method for the processing of doped spinels. The Fe-doped coatings demonstrated a lower parabolic oxidation rate and thinner oxide scale in comparison with both the undoped $Mn_{1,5}Co_{1,5}O_4$ spinel coating and bare Crofer 22 APU. The best protection was achieved with the 10FeMCO_R1000 coating, due to the combined beneficial effect of Fe-doping and a higher temperature of the reducing step (1000°C instead of 900°C). The higher temperature promoted greater densification of the coating and better pre-oxidation of the steel substrate.

References

[1] M.P. Carpanese, M. Panizza, M. Viviani, E. Mercadelli, A. Sanson, A. Barbucci, Study of reversible SOFC/SOEC based on a mixed anionic-protonic conductor, J. Appl. Electrochem. 45 (2015) 657–665. https://doi.org/10.1007/s10800-015-0838-8.

[2] O.Z. Sharaf, M.F. Orhan, An overview of fuel cell technology: Fundamentals and applications, Renew. Sustain. Energy Rev. 32 (2014) 810–853. https://doi.org/10.1016/j.rser.2014.01.012.

[3] W.Z. Zhu, S.C. Deevi, Development of interconnect materials for solid oxide fuel cells, Mater. Sci. Eng. A. 348 (2003) 227–243. https://doi.org/10.1016/S0921-5093(02)00736-0.

[4] F.S. da Silva, T.M. de Souza, Novel materials for solid oxide fuel cell technologies: A literature review, Int. J. Hydrogen Energy. 42 (2017) 26020–26036. https://doi.org/10.1016/j.ijhydene.2017.08.105.

[5] N. Mahato, A. Banerjee, A. Gupta, S. Omar, K. Balani, Progress in material selection for solid oxide fuel cell technology: A review, Prog. Mater. Sci. 72 (2015) 141–337. https://doi.org/10.1016/j.pmatsci.2015.01.001.

[6] A. Nakajo, J. Kuebler, A. Faes, U.F. Vogt, H.J. Schindler, L.-K.K. Chiang, S. Modena, J. Van herle, T. Hocker, Compilation of mechanical properties for the structural analysis of solid oxide fuel cell stacks. Constitutive materials of anode-supported cells, Ceram. Int. 38 (2012) 3907–3927.

https://doi.org/10.1016/j.ceramint.2012.01.043.
[7] P. Kofstad, R. Bredesen, High temperature corrosion in SOFC environments, Solid State Ionics. 52 (1992) 69–75. https://doi.org/10.1016/0167-2738(92)90092-4.
[8] J.W. Fergus, Metallic interconnects for solid oxide fuel cells, Mater. Sci. Eng. A. 397 (2005) 271–283. https://doi.org/10.1016/j.msea.2005.02.047.
[9] Z. Yang, Recent advances in metallic interconnects for solid oxide fuel cells, Int. Mater. Rev. 53 (2008) 39–54. https://doi.org/10.1179/174328007X212526.
[10] VDM-Metals, VDM ® Crofer 22 APU, (2010). https://www.vdm-metals.com/fileadmin/user_upload/Downloads/Data_Sheets/Datenblatt_VDM_Crofer_22_APU.pdf (accessed April 2, 2019).
[11] M. Palcut, L. Mikkelsen, K. Neufeld, M. Chen, R. Knibbe, P. V. Hendriksen, Corrosion stability of ferritic stainless steels for solid oxide electrolyser cell interconnects, Corros. Sci. 52 (2010) 3309–3320. https://doi.org/10.1016/j.corsci.2010.06.006.
[12] R. Sachitanand, M. Sattari, J.E. Svensson, J. Froitzheim, Evaluation of the oxidation and Cr evaporation properties of selected FeCr alloys used as SOFC interconnects, Int. J. Hydrogen Energy. 38 (2013) 15328–15334. https://doi.org/10.1016/j.ijhydene.2013.09.044.
[13] P. Huczkowski, S. Ertl, J. Piron-Abellan, N. Christiansen, T. Höfler, V. Shemet, L. Singheiser, W.J. Quadakkers, Effect of component thickness on lifetime and oxidation rate of chromia forming ferritic steels in low and high pO2environments, Mater. High Temp. 22 (2005) 253–262. https://doi.org/10.1179/mht.2005.029.
[14] W.Z. Zhu, S.C. Deevi, Opportunity of metallic interconnects for solid oxide fuel cells: A status on contact resistance, Mater. Res. Bull. 38 (2003) 957–972. https://doi.org/10.1016/S0025-5408(03)00076-X.
[15] K. Wang, Y. Liu, J.W. Fergus, Interactions between SOFC interconnect coating materials and chromia, J. Am. Ceram. Soc. 94 (2011) 4490–4495. https://doi.org/10.1111/j.1551-2916.2011.04749.x.
[16] J.W. Fergus, Effect of cathode and electrolyte transport properties on chromium poisoning in solid oxide fuel cells, Int. J. Hydrogen Energy. 32 (2007) 3664–3671. https://doi.org/10.1016/j.ijhydene.2006.08.005.
[17] H. Falk-Windisch, J.E. Svensson, J. Froitzheim, The effect of temperature on chromium vaporization and oxide scale growth on interconnect steels for Solid Oxide Fuel Cells, J. Power Sources. 287 (2015) 25–35. https://doi.org/10.1016/j.jpowsour.2015.04.040.
[18] M. Stanislowski, J. Froitzheim, L. Niewolak, W.J. Quadakkers, K. Hilpert, T. Markus, L. Singheiser, Reduction of chromium vaporization from SOFC interconnectors by highly effective coatings, J. Power Sources. 164 (2007) 578–589. https://doi.org/10.1016/j.jpowsour.2006.08.013.
[19] N. Shaigan, W. Qu, D.G. Ivey, W. Chen, A review of recent progress in coatings, surface modifications and alloy developments for solid oxide fuel cell ferritic stainless steel interconnects, J. Power Sources. 195 (2010) 1529–1542. https://doi.org/10.1016/j.jpowsour.2009.09.069.
[20] J.C.W. Mah, A. Muchtar, M.R. Somalu, M.J. Ghazali, Metallic interconnects for solid oxide fuel cell: A review on protective coating and deposition techniques, Int. J. Hydrogen Energy. 42 (2017) 9219–9229. https://doi.org/10.1016/j.ijhydene.2016.03.195.
[21] N. Orlovskaya, A. Coratolo, C. Johnson, R. Gemmen, Structural

Characterization of Lanthanum Chromite Perovskite Coating Deposited by Magnetron Sputtering on an Iron-Based Chromium-Containing Alloy as a Promising Interconnect Material for SOFCs, J. Am. Ceram. Soc. 87 (2005) 1981–1987. https://doi.org/10.1111/j.1151-2916.2004.tb06350.x.
[22] S. Fontana, R. Amendola, S. Chevalier, P. Piccardo, G. Caboche, M. Viviani, R. Molins, M. Sennour, Metallic interconnects for SOFC: Characterisation of corrosion resistance and conductivity evaluation at operating temperature of differently coated alloys, J. Power Sources. 171 (2007) 652–662. https://doi.org/10.1016/j.jpowsour.2007.06.255.
[23] Y.-Y. Chang, C.-P. Chang, D.-Y. Wang, S.-M. Yang, W. Wu, High temperature oxidation resistance of CrAlSiN coatings synthesized by a cathodic arc deposition process, J. Alloys Compd. 461 (2008) 336–341. https://doi.org/10.1016/j.jallcom.2007.06.084.
[24] Y. Larring, T. Norby, Spinel and Perovskite Functional Layers Between Plansee Metallic Interconnect (Cr-5 wt % Fe-1 wt % Y[sub 2]O[sub 3]) and Ceramic (La[sub 0.85]Sr[sub 0.15])[sub 0.91]MnO[sub 3] Cathode Materials for Solid Oxide Fuel Cells, J. Electrochem. Soc. 147 (2000) 3251. https://doi.org/10.1149/1.1393891.
[25] F. Smeacetto, A. De Miranda, S. Cabanas Polo, S. Molin, D. Boccaccini, M. Salvo, A.R. Boccaccini, Electrophoretic deposition of Mn1.5Co1.5O4 on metallic interconnect and interaction with glass-ceramic sealant for solid oxide fuel cells application, J. Power Sources. 280 (2015) 379–386. https://doi.org/10.1016/j.jpowsour.2015.01.120.
[26] A. Masi, M. Bellusci, S.J. McPhail, F. Padella, P. Reale, J.E. Hong, R. Steinberger-Wilckens, M. Carlini, Cu-Mn-Co oxides as protective materials in SOFC technology: The effect of chemical composition on mechanochemical synthesis, sintering behaviour, thermal expansion and electrical conductivity, J. Eur. Ceram. Soc. 37 (2017) 661–669. https://doi.org/10.1016/j.jeurceramsoc.2016.09.025.
[27] M. Bobruk, K. Brylewska, K. Durczak, K. Wojciechowski, A. Adamczyk, T. Brylewski, Synthesis of manganese-cobalt spinel via wet chemistry methods and its properties, Ceram. Int. 43 (2017) 15597–15609. https://doi.org/10.1016/j.ceramint.2017.08.116.
[28] H. Bordeneuve, C. Tenailleau, S. Guillemet-Fritsch, R. Smith, E. Suard, A. Rousset, Structural variations and cation distributions in Mn3-xCoxO4(0 ≤ x ≤ 3) dense ceramics using neutron diffraction data, Solid State Sci. 12 (2010) 379–386. https://doi.org/10.1016/j.solidstatesciences.2009.11.018.
[29] X. Chen, P.Y. Hou, C.P. Jacobson, S.J. Visco, L.C. De Jonghe, Protective coating on stainless steel interconnect for SOFCs: Oxidation kinetics and electrical properties, Solid State Ionics. 176 (2005) 425–433. https://doi.org/10.1016/j.ssi.2004.10.004.
[30] Z. Yang, G.G. Xia, X.H. Li, J.W. Stevenson, (Mn,Co)3O4 spinel coatings on ferritic stainless steels for SOFC interconnect applications, Int. J. Hydrogen Energy. 32 (2007) 3648–3654. https://doi.org/10.1016/j.ijhydene.2006.08.048.
[31] L. Chen, E.Y. Sun, J. Yamanis, N. Magdefrau, Oxidation Kinetics of Mn 1.5Co1.5O4-Coated Haynes 230 and Crofer 22 APU for Solid Oxide Fuel Cell Interconnects, J. Electrochem. Soc. 157 (2010) B931. https://doi.org/10.1149/1.3391820.
[32] T. Brylewski, W. Kucza, A. Adamczyk, A. Kruk, M. Stygar, M. Bobruk, J. Dąbrowa, Microstructure and electrical properties of Mn1+xCo2−xO4 (0≤x≤1.5)

spinels synthesized using EDTA-gel processes, Ceram. Int. 40 (2014) 13873–13882. https://doi.org/10.1016/j.ceramint.2014.05.106.
[33] S. Molin, A.G. Sabato, M. Bindi, P. Leone, G. Cempura, M. Salvo, S. Cabanas Polo, A.R. Boccaccini, F. Smeacetto, Microstructural and electrical characterization of Mn-Co spinel protective coatings for solid oxide cell interconnects, J. Eur. Ceram. Soc. 37 (2017) 4781–4791. https://doi.org/10.1016/j.jeurceramsoc.2017.07.011.
[34] S.-I. Lee, J. Hong, H. Kim, J.-W. Son, J.-H. Lee, B.-K. Kim, H.-W. Lee, K.J. Yoon, Highly Dense Mn-Co Spinel Coating for Protection of Metallic Interconnect of Solid Oxide Fuel Cells, J. Electrochem. Soc. 161 (2014) F1389–F1394. https://doi.org/10.1149/2.0541414jes.
[35] A. Kruk, M. Stygar, T. Brylewski, Mn–Co spinel protective–conductive coating on AL453 ferritic stainless steel for IT-SOFC interconnect applications, J. Solid State Electrochem. 17 (2013) 993–1003. https://doi.org/10.1007/s10008-012-1952-8.
[36] V.I. Gorokhovsky, P.E. Gannon, M.C. Deibert, R.J. Smith, A. Kayani, M. Kopczyk, D. VanVorous, Z. Yang, J.W. Stevenson, S. Visco, C. Jacobson, H. Kurokawa, S.W. Sofie, Deposition and Evaluation of Protective PVD Coatings on Ferritic Stainless Steel SOFC Interconnects, J. Electrochem. Soc. 153 (2006) A1886. https:///doi.org/10.1149/1.2266244.
[37] C.C. Mardare, M. Spiegel, A. Savan, A. Ludwig, Thermally Oxidized Mn–Co Thin Films as Protective Coatings for SOFC Interconnects, J. Electrochem. Soc. 156 (2009) B1431. https://doi.org/10.1149/1.3240597.
[38] H.H. Zhang, C.L. Zeng, Preparation and performances of Co–Mn spinel coating on a ferritic stainless steel interconnect material for solid oxide fuel cell application, J. Power Sources. 252 (2014) 122–129. https://doi.org/10.1016/j.jpowsour.2013.12.007.
[39] S.J. Han, Z. Pala, S. Sampath, Plasma sprayed manganese–cobalt spinel coatings: Process sensitivity on phase, electrical and protective performance, J. Power Sources. 304 (2016) 234–243. https://doi.org/10.1016/j.jpowsour.2015.11.040.
[40] L. Besra, M. Liu, A review on fundamentals and applications of electrophoretic deposition (EPD), Prog. Mater. Sci. 52 (2007) 1–61. https://doi.org/10.1016/j.pmatsci.2006.07.001.
[41] M. Bobruk, S. Molin, M. Chen, T. Brylewski, P.V. Hendriksen, Sintering of MnCo2O4coatings prepared by electrophoretic deposition, Mater. Lett. 213 (2018) 394–398. https://doi.org/10.1016/j.matlet.2017.12.046.
[42] H. Zhang, Z. Zhan, X. Liu, Electrophoretic deposition of (Mn,Co)3O4 spinel coating for solid oxide fuel cell interconnects, J. Power Sources. 196 (2011) 8041–8047. https://doi.org/10.1016/j.jpowsour.2011.05.053.
[43] M. Mirzaei, A. Simchi, M.A. Faghihi-Sani, A. Yazdanyar, Electrophoretic deposition and sintering of a nanostructured manganese-cobalt spinel coating for solid oxide fuel cell interconnects, Ceram. Int. 42 (2016) 6648–6656. https://doi.org/10.1016/j.ceramint.2016.01.012.
[44] B. Talic, H. Falk-Windisch, V. Venkatachalam, P.V. Hendriksen, K. Wiik, H.L. Lein, Effect of coating density on oxidation resistance and Cr vaporization from solid oxide fuel cell interconnects, J. Power Sources. 354 (2017) 57–67. https://doi.org/10.1016/j.jpowsour.2017.04.023.
[45] L. V. Gambino, N.J. Magdefrau, M. Aindow, Microstructural effects of the reduction step in reactive consolidation of manganese cobaltite coatings on

Crofer 22 APU, Mater. High Temp. 32 (2015) 142–147. https://doi.org/10.1179/0960340914Z.00000000090.
[46] S.R. Akanda, N.J. Kidner, M.E. Walter, Spinel coatings on metallic interconnects: Effect of reduction heat treatment on performance, Surf. Coatings Technol. 253 (2014) 255–260. https://doi.org/10.1016/j.surfcoat.2014.05.049.
[47] J.W. Fergus, K. Wang, Y. Liu, Transition Metal Spinel Oxide Coatings for Reducing Chromium Poisoning in SOFCs, in: 2011: pp. 77–84. https://doi.org/10.1149/1.3589187.
[48] B. Talic, S. Molin, K. Wiik, P.V. Hendriksen, H.L. Lein, Comparison of iron and copper doped manganese cobalt spinel oxides as protective coatings for solid oxide fuel cell interconnects, J. Power Sources. 372 (2017) 145–156. https://doi.org/10.1016/j.jpowsour.2017.10.060.
[49] B. Talic, P.V. Hendriksen, K. Wiik, H.L. Lein, Thermal expansion and electrical conductivity of Fe and Cu doped MnCo2O4spinel, Solid State Ionics. 326 (2018) 90–99. https://doi.org/10.1016/j.ssi.2018.09.018.
[50] A. Masi, M. Bellusci, S.J. McPhail, F. Padella, P. Reale, J.-E. Hong, R. Steinberger-Wilckens, M. Carlini, The effect of chemical composition on high temperature behaviour of Fe and Cu doped Mn-Co spinels, Ceram. Int. 43 (2016) 2829–2835. https://doi.org/10.1016/j.ceramint.2016.11.135.
[51] N. Grünwald, Y.J. Sohn, X. Yin, N.H. Menzler, O. Guillon, R. Vaßen, Microstructure and phase evolution of atmospheric plasma sprayed Mn-Co-Fe oxide protection layers for solid oxide fuel cells, J. Eur. Ceram. Soc. 39 (2019) 449–460. https://doi.org/10.1016/j.jeurceramsoc.2018.08.027.
[52] S. Molin, P. Jasinski, L. Mikkelsen, W. Zhang, M. Chen, P. V. Hendriksen, Low temperature processed MnCo2O4and MnCo1.8Fe0.2O4 as effective protective coatings for solid oxide fuel cell interconnects at 750 °C, J. Power Sources. 336 (2016) 408–418. https://doi.org/10.1016/j.jpowsour.2016.11.011.
[53] J. Puranen, M. Pihlatie, J. Lagerbom, G. Bolelli, J. Laakso, L. Hyvärinen, M. Kylmälahti, O. Himanen, J. Kiviaho, L. Lusvarghi, P. Vuoristo, Post-mortem evaluation of oxidized atmospheric plasma sprayed Mn-Co-Fe oxide spinel coatings on SOFC interconnectors, Int. J. Hydrogen Energy. 39 (2014) 17284–17294. https://doi.org/10.1016/j.ijhydene.2014.08.105.
[54] J. Puranen, J. Lagerbom, L. Hyvärinen, M. Kylmälahti, O. Himanen, M. Pihlatie, J. Kiviaho, P. Vuoristo, The structure and properties of plasma sprayed iron oxide doped manganese cobalt oxide spinel coatings for SOFC metallic interconnectors, J. Therm. Spray Technol. 20 (2011) 154–159. https://doi.org/10.1007/s11666-010-9598-5.
[55] M. Bednarz, S. Molin, M. Bobruk, M. Stygar, E. Długoń, M. Sitarz, T. Brylewski, High-temperature oxidation of the Crofer 22 H ferritic steel with Mn1.45Co1.45Fe0.1O4 and Mn1.5Co1.5O4 spinel coatings under thermal cycling conditions and its properties, Mater. Chem. Phys. 225 (2019) 227–238. https://doi.org/10.1016/j.matchemphys.2018.12.090.
[56] S. Molin, A.G. Sabato, H. Javed, G. Cempura, A.R. Boccaccini, F. Smeacetto, Co-deposition of CuO and Mn 1.5Co1.5 O4 powders on Crofer22APU by electrophoretic method: Structural, compositional modifications and corrosion properties, Mater. Lett. 218 (2018) 329–333. https://doi.org/10.1016/j.matlet.2018.02.037.
[57] S. Bhattacharjee, DLS and zeta potential – What they are and what they are not?, J. Control. Release. 235 (2016) 337–351.

https://doi.org/10.1016/j.jconrel.2016.06.017.
[58] J.G. Grolig, Coated Ferritic Stainless Steels as Interconnects in Solid Oxide Fuel Cells, 2013. https://publications.lib.chalmers.se/publication/184010-coated-ferritic-stainless-steels-as-interconnects-in-solid-oxide-fuel-cells.
[59] C.A. Schneider, W.S. Rasband, K.W. Eliceiri, NIH Image to ImageJ: 25 years of image analysis, Nat. Methods. 9 (2012) 671–675. https://doi.org/10.1038/nmeth.2089.
[60] A. Mikolajczyk, A. Gajewicz, B. Rasulev, N. Schaeublin, E. Maurer-gardner, S. Hussain, J. Leszczynski, T. Puzyn, Zeta Potential for Metal Oxide Nanoparticles: A Predictive Model Developed by a Nano-Quantitative Structure − Property Relationship Approach, Chem. Mater. 27 (2015) 2400–2407. https://doi.org/10.1021/cm504406a.
[61] I. Corni, N. Neumann, S. Novak, K. König, P. Veronesi, Q. Chen, M.P. Ryan, A.R. Boccaccini, Electrophoretic deposition of PEEK-nano alumina composite coatings on stainless steel, Surf. Coatings Technol. 203 (2009) 1349–1359. https://doi.org/10.1016/j.surfcoat.2008.11.005.
[62] D.J. Young, High Temperature Oxidation and Corrosion of Metals, volume 1, Elsevier, 2008. https://doi.org/10.1016/C2014-0-00259-6.
[63] W.N. Liu, X. Sun, E. Stephens, M.A. Khaleel, Life prediction of coated and uncoated metallic interconnect for solid oxide fuel cell applications, J. Power Sources. 189 (2009) 1044–1050. https://doi.org/10.1016/j.jpowsour.2008.12.143.
[64] M. Stanislowski, E. Wessel, K. Hilpert, T. Markus, L. Singheiser, Chromium Vaporization from High-Temperature Alloys, J. Electrochem. Soc. 154 (2007) A295. https://doi.org/10.1149/1.2434690.
[65] B. Talic, P.V. Hendriksen, K. Wiik, H.L. Lein, Diffusion couple study of the interaction between Cr2O3 and MnCo2O4 doped with Fe and Cu, Solid State Ionics. 332 (2019) 16–24. https://doi.org/10.1016/j.ssi.2019.01.008.
[66] B. Talic, S. Molin, P.V. Hendriksen, H.L. Lein, Effect of pre-oxidation on the oxidation resistance of Crofer 22 APU, Corros. Sci. 138 (2018) 189–199. https://doi.org/10.1016/j.corsci.2018.04.016.
[67] N.J. Magdefrau, L. Chen, E.Y. Sun, M. Aindow, Effects of alloy heat treatment on oxidation kinetics and scale morphology for crofer 22 APU, J. Power Sources. 241 (2013) 756–767. https://doi.org/10.1016/j.jpowsour.2013.03.181.

Table 1

Sample name	EPD suspension	Two-step sintering	Coating theoretical composition
MCO	100wt.% $Mn_{1.5}Co_{1.5}O_4$	900°C, 2h, Ar/H_2 900°C, 2h, air	$Mn_{1,5}Co_{1,5}O_4$
5FeMCO	95wt.% $Mn_{1.5}Co_{1.5}O_4$ 5wt.% Fe_2O_3	900°C, 2h, Ar/H_2 900°C, 2h, air	$Mn_{1,43}Co_{1,43}Fe_{0,14}O_4$
10FeMCO	90wt.% $Mn_{1.5}Co_{1.5}O_4$ 10wt.% Fe_2O_3	900°C, 2h, Ar/H_2 900°C, 2h, air	$Mn_{1,35}Co_{1,35}Fe_{0,30}O_4$
10FeMCO_R1000	90wt.% $Mn_{1.5}Co_{1.5}O_4$ 10wt.% Fe_2O_3	1000°C, 2h, Ar/H_2 900°C, 2h, air	$Mn_{1,35}Co_{1,35}Fe_{0,30}O_4$

Table 2

Sample	Mass gain [mg cm^{-2}]	$k_{p,m}$ [g^2 cm^{-4} s^{-1}]	Oxide scale [µm]
Uncoated Crofer 22 APU	0.41 ± 0.05	26.9×10^{-15}	2.5 ± 0.3
MCO	0.29 ± 0.03	14.5×10^{-15}	1.8 ± 0.1
5FeMCO	0.20 ± 0.02	6.6×10^{-15}	1.2 ± 0.1
10FeMCO	0.20 ± 0.02	6.6×10^{-15}	1.2 ± 0.1
10FeMCO_R1000	0.14 ± 0.03	3.3×10^{-15}	0.8 ± 0.2

Table 3

Sample	Oxide scale [µm]	
	Measured	Calculated
MCO	1.1 ± 0.1	1.8 ± 0.1
5FeMCO	0.8 ± 0.1	1.2 ± 0.1
10FeMCO	0.6 ± 0.2	1.2 ± 0.1
10FeMCO_R1000	0.7 ± 0.2	0.8 ± 0.2

Figure 1

Click here to download high resolution image

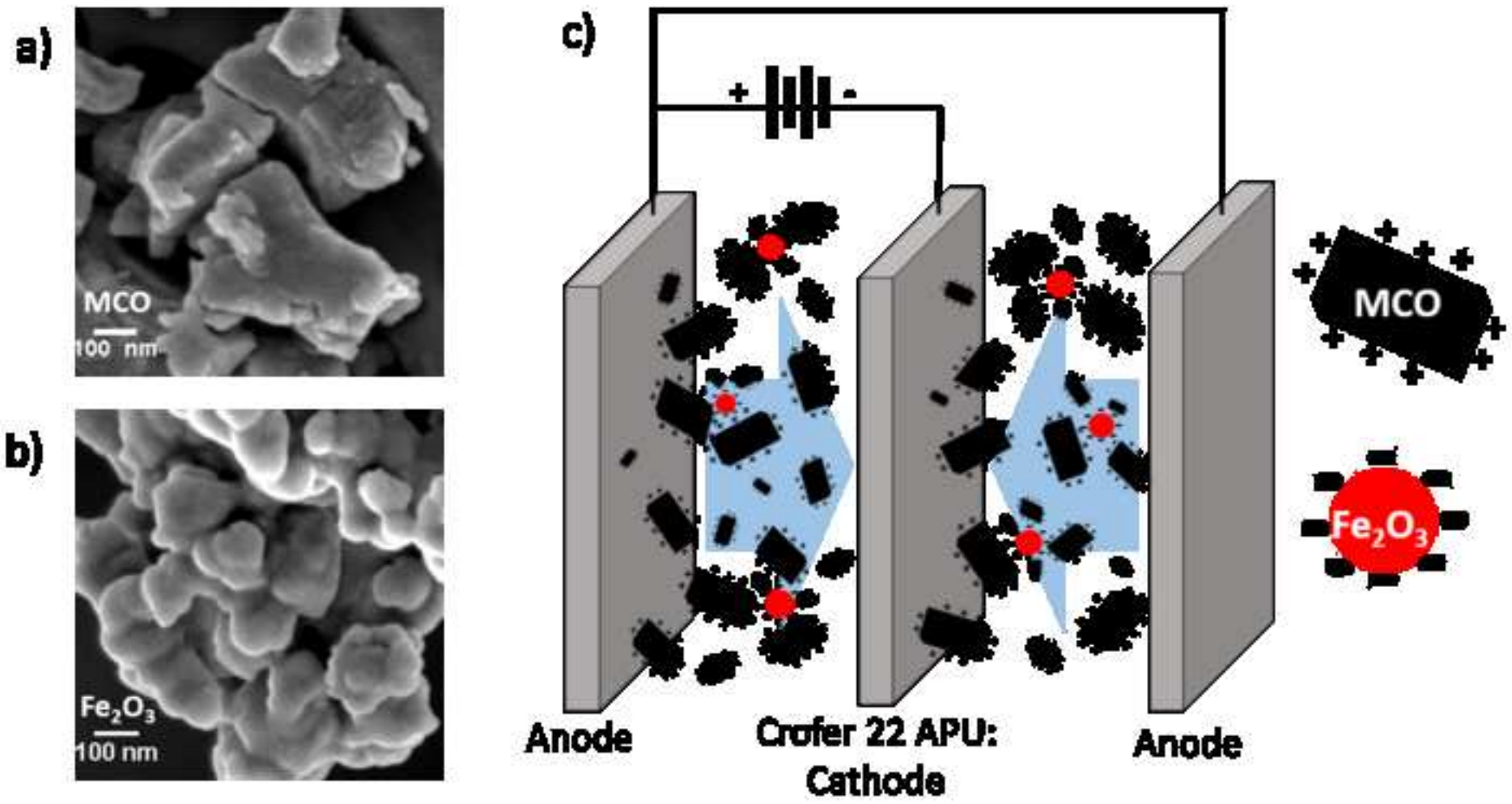

Figure 2

Click here to download high resolution image

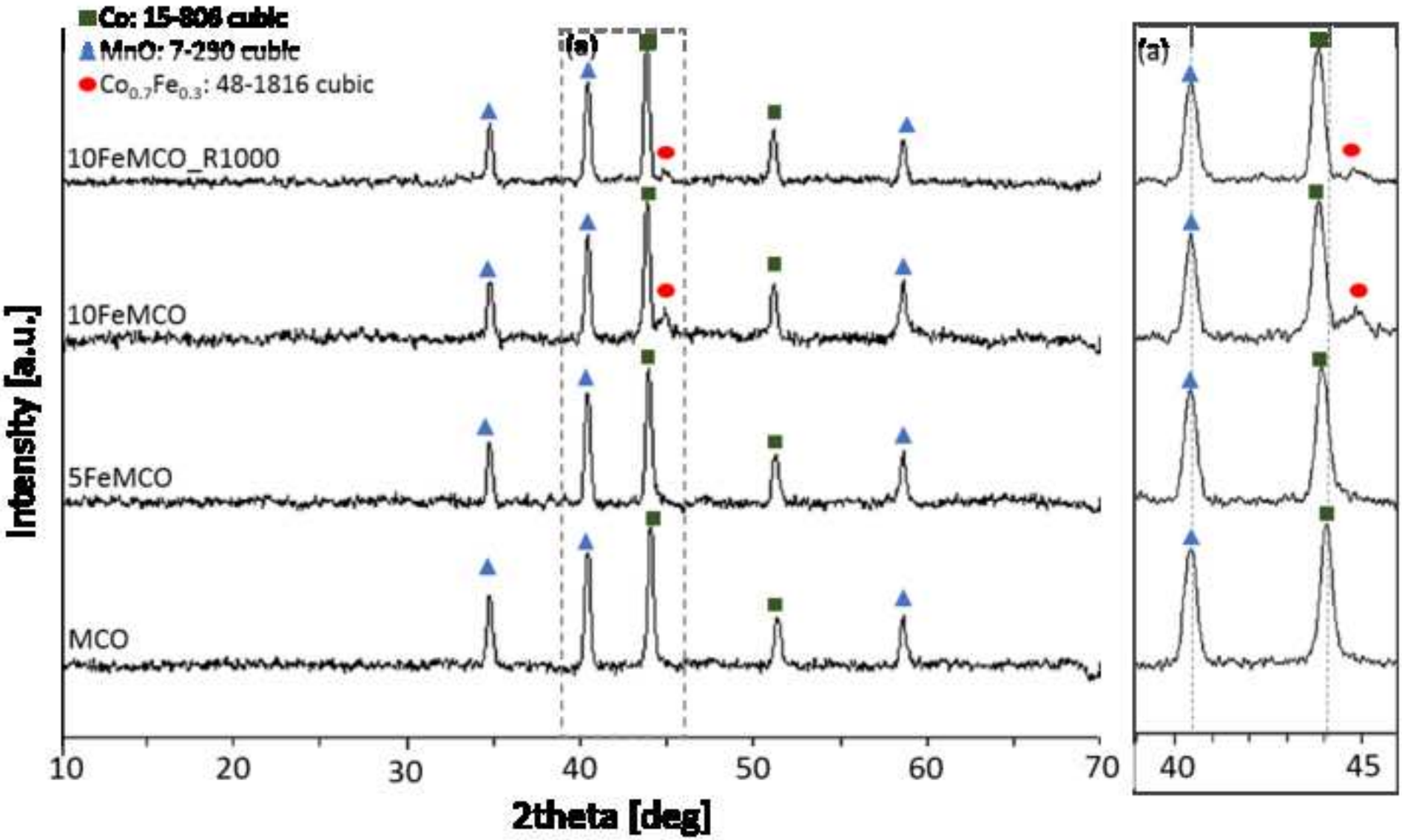

Figure 3

Click here to download high resolution image

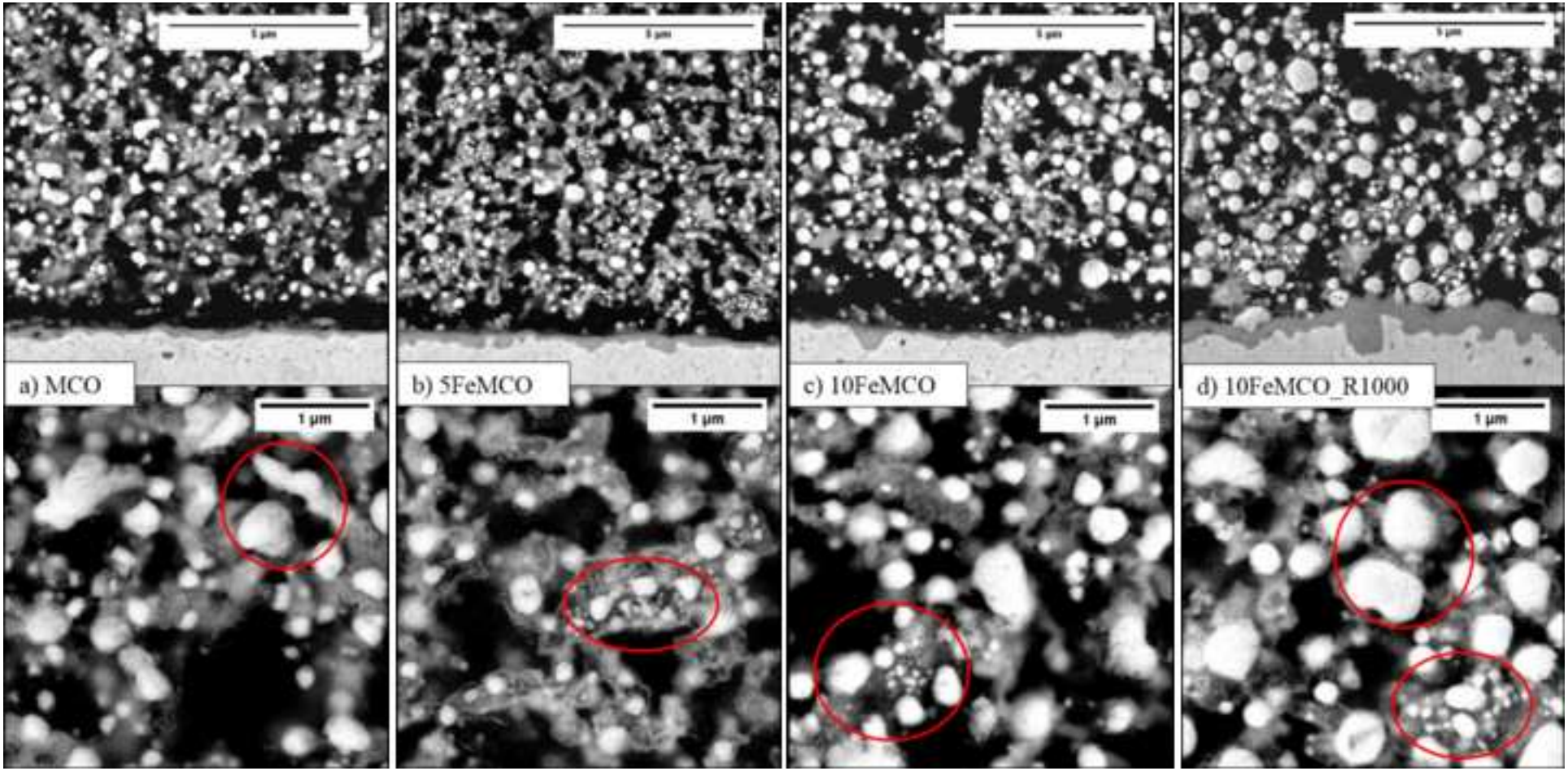

Figure 4

Click here to download high resolution image

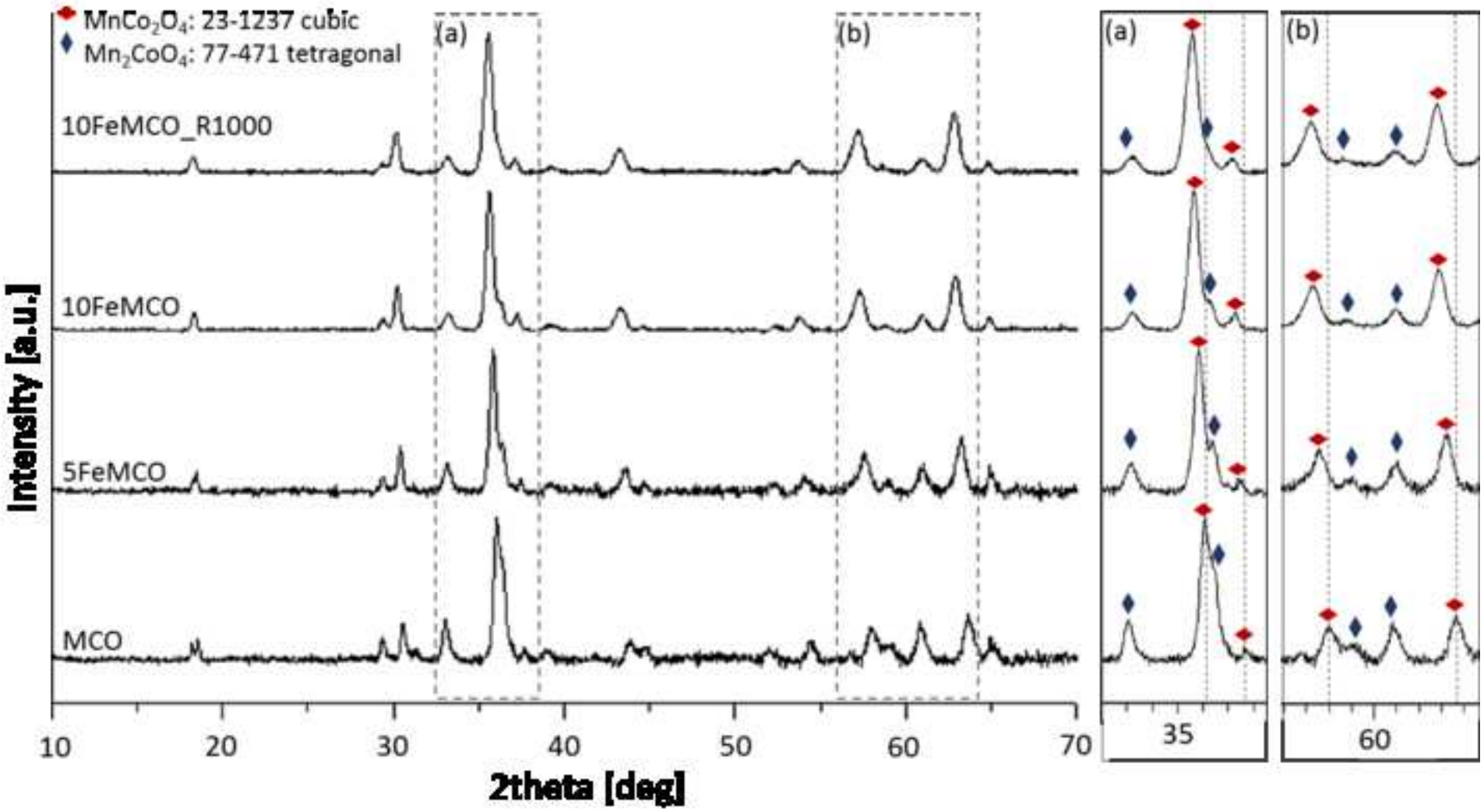

Figure 5

Click here to download high resolution image

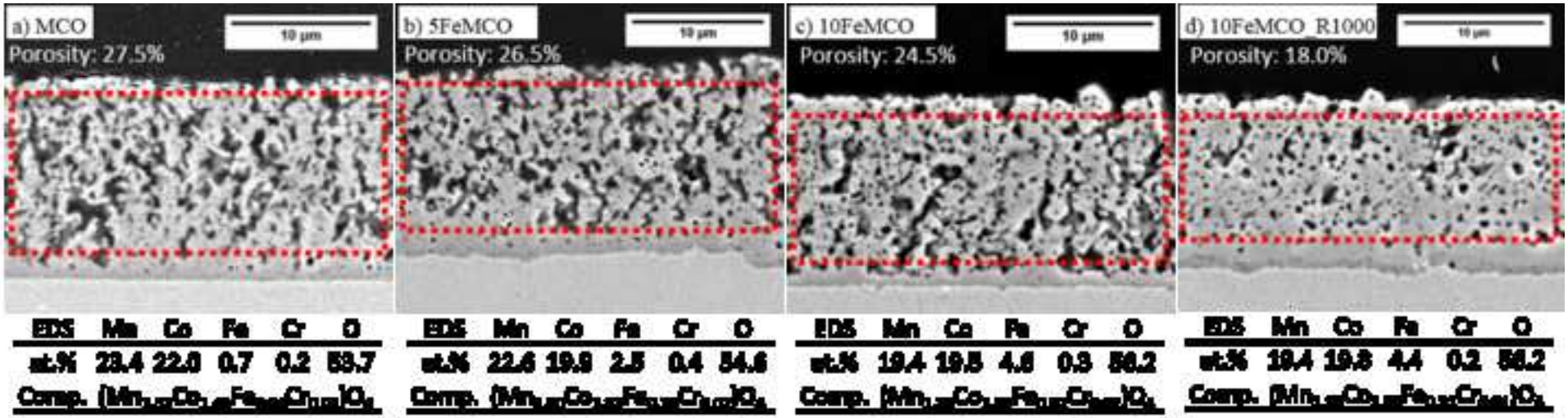

Figure 6

Click here to download high resolution image

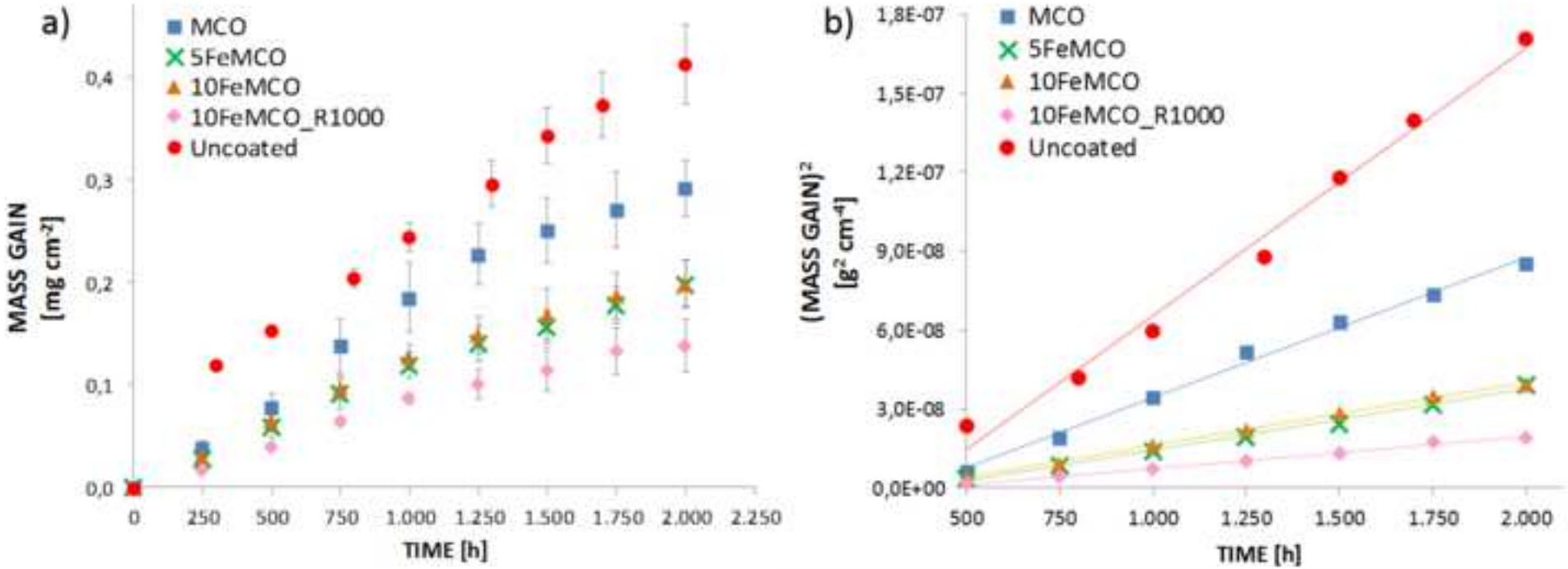

Figure 7

Click here to download high resolution image

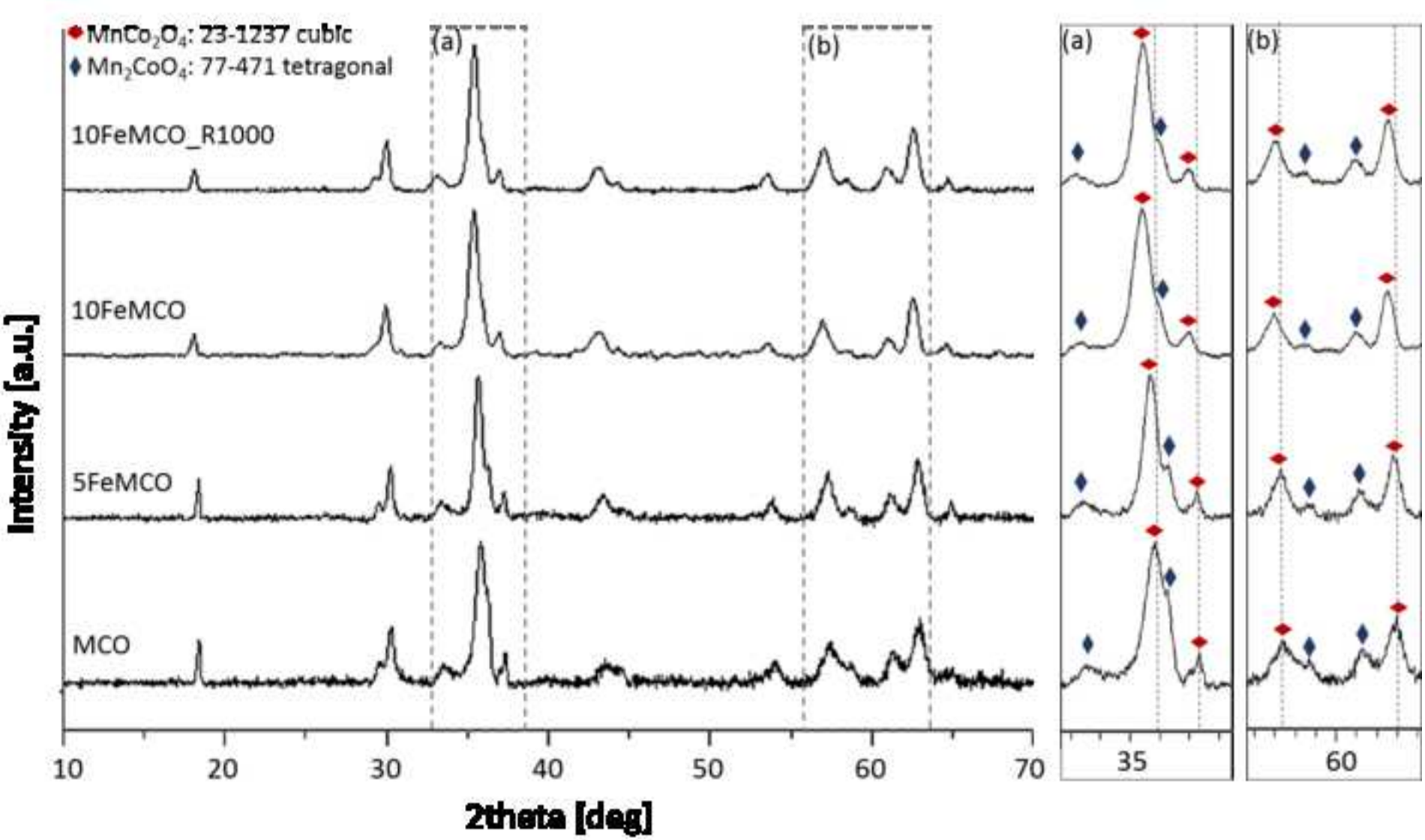

Figure 8

Click here to download high resolution image

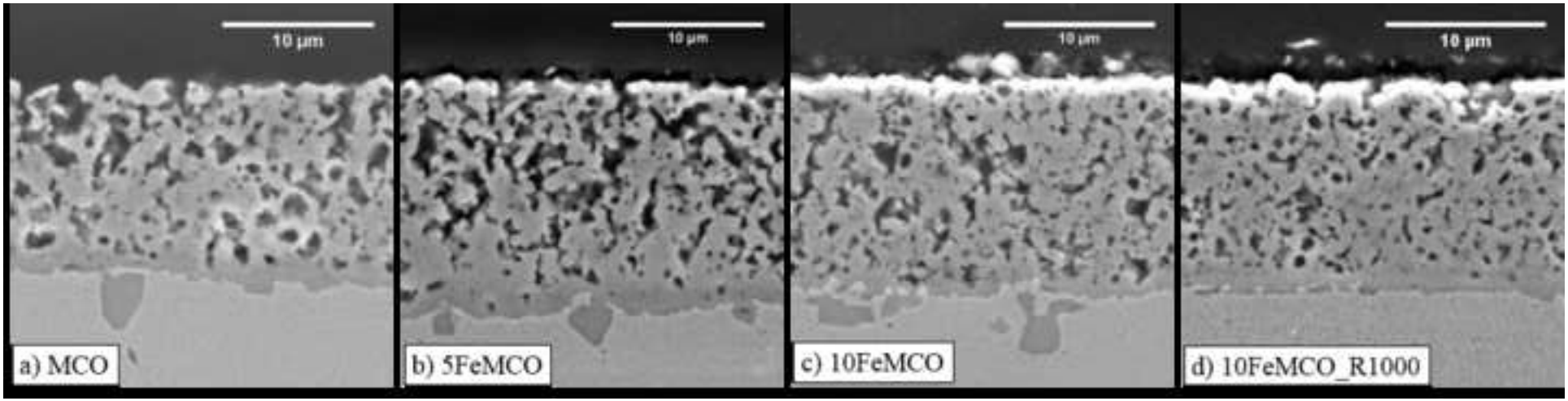

Figure 9

Click here to download high resolution image

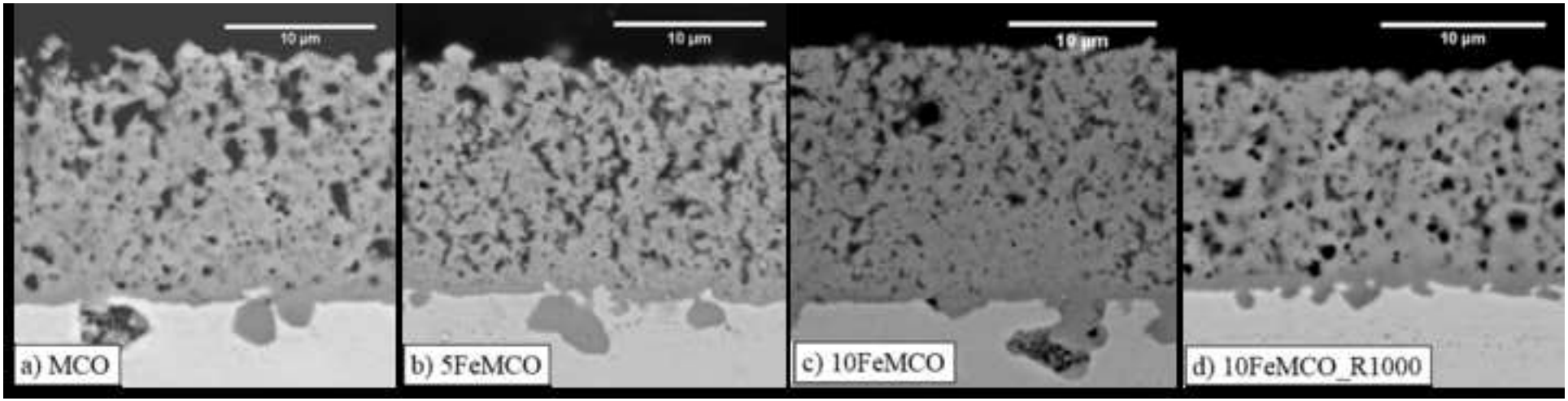

Figure 10

Click here to download high resolution image

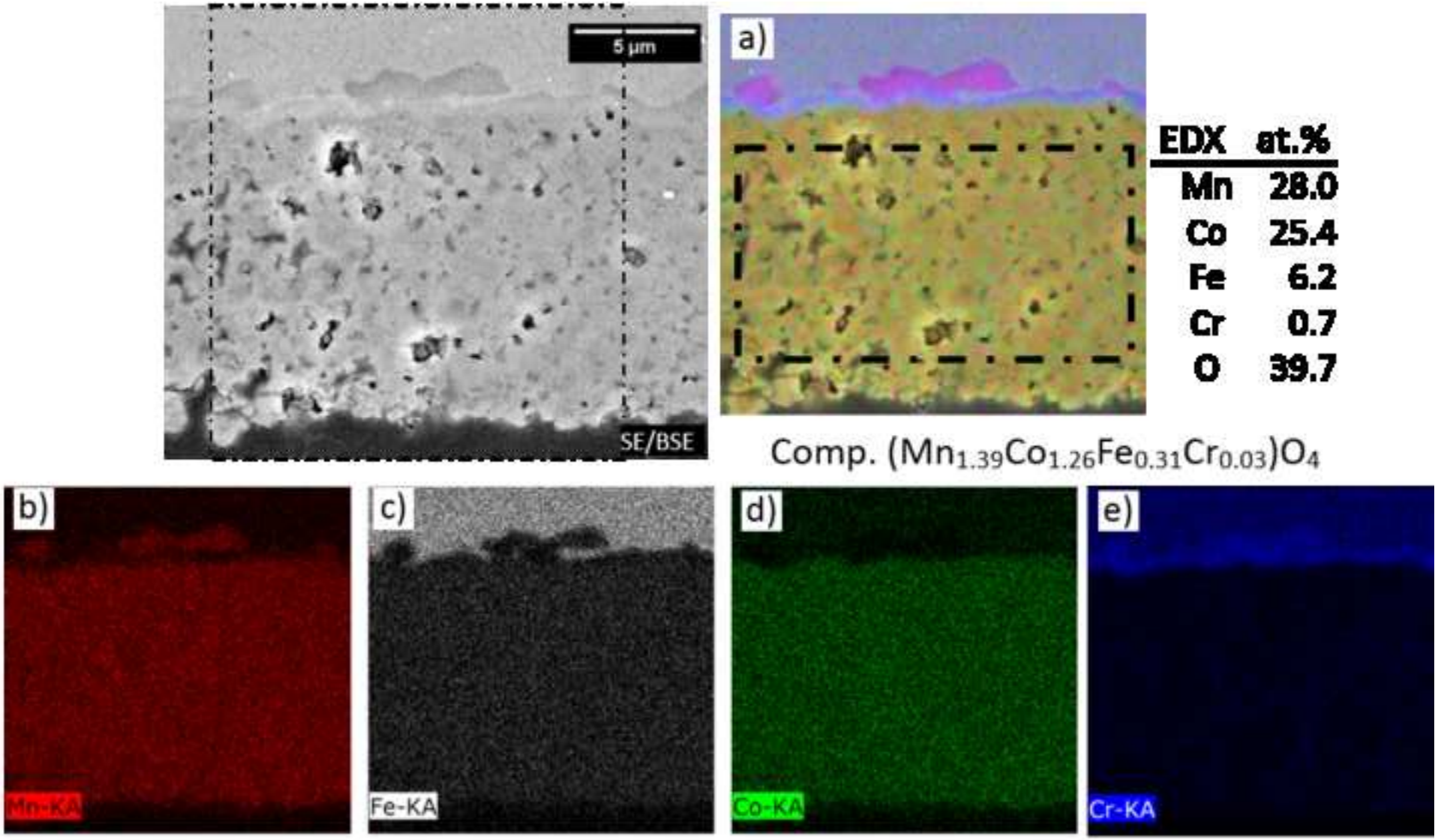

Figure 11
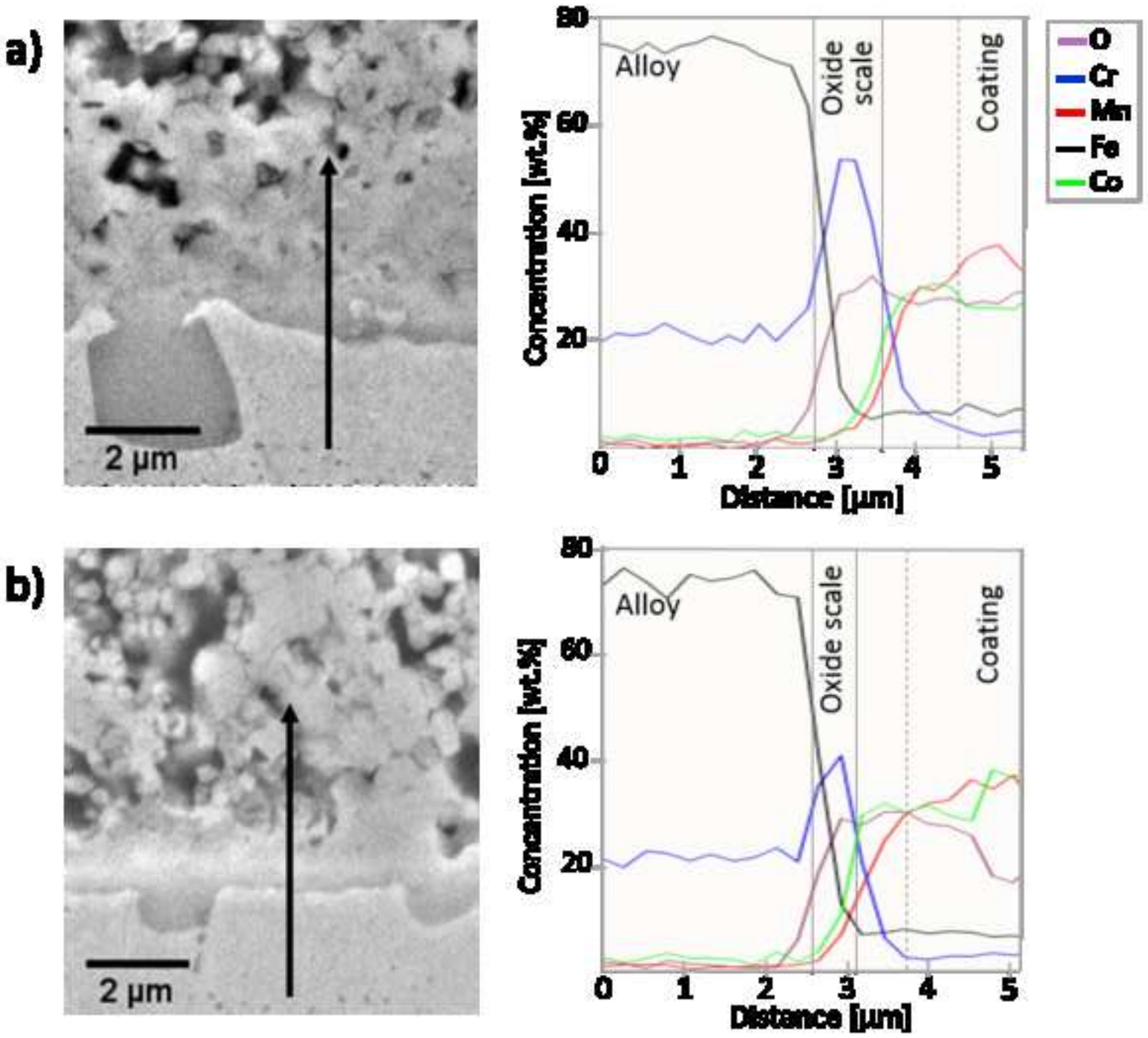
Click here to download high resolution image